AMAS WORKSHOP ON ORTHOPAEDIC BIOMECHANICS
OBM'02 – (PP.333–382) – WROCŁAW, SEPTEMBER 1-4, 2002.

Homogenization methods in bone mechanics

J. J. TELEGA, A. GAŁKA, B. GAMBIN,
and S. TOKARZEWSKI

Institute of Fundamental Technological Research
Świętokrzyska 21, 00-049 Warszawa, Poland
jtelega@ippt.gov.pl

The aim of the paper is threefold. First, available results on finding the effective macroscopic elastic moduli of compact bone by using homogenization are reviewed. It is shown that proper framework for studying such biological materials with hierarchical microstructure is that of reiterated homogenization. Γ-convergence theory is applied to obtain general formulae for the effective elastic moduli of a material with three structural levels. Second, effective models of cancellous bone with various architectures are overviewed. Third, influence of marrow on torsional behavior of long bone is discussed.

1. Introduction

Bones occur in two forms: as a dense solid *(compact bone)* and as a porous network of connecting rods and plates *(cancellous or trabecular bone)*. The

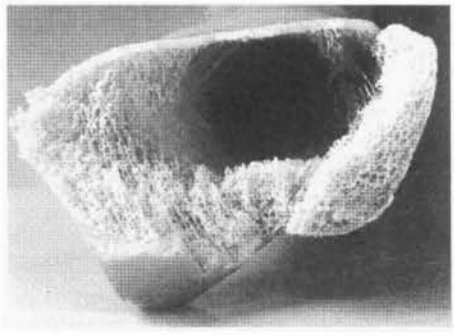

FIGURE 1. Photograph of proximal part of the human femur, after Gałka *et al.* [37].

most obvious difference between these two types of bones appears in their relative densities measured by volume fractions of solids, cf. Fig. 1.

Bone with a volume fraction of less than 70% is classified as cancellous while that over 70% is compact, cf. [39]. Most bones in the body are of both types, the dense compact bone forming an outer shell surrounding a core of spongy cancellous bone, cf. Fig. 2. In this paper we summarize the results of modeling both compact and cancellous bone by using homogenization methods.

Bone cells produce two types of tissue, the well-organized lamellar bone and the poorly organized woven bone. When lamellar bone occurs in the

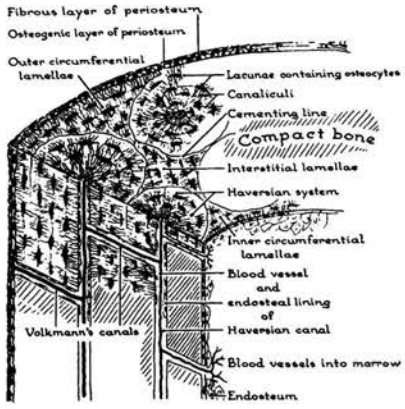

FIGURE 2. The basic structure of compact bone, after [29].

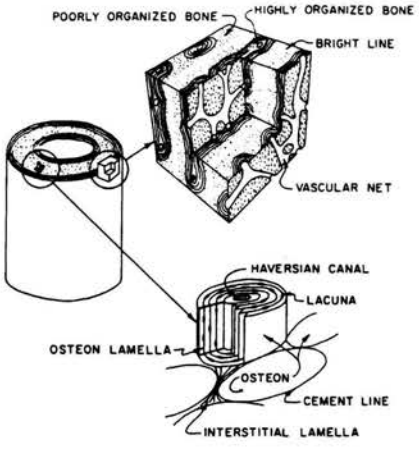

FIGURE 3. Typical bone structure in the diaphysis of the femur, after Cowin [29].

midshaft of a long bone, it consists of concentrically arranged laminae as illustrated in Fig. 3.

The thickness of the lamina is about 200 μm. Between each lamina and the next there is a net-like system of blood vessels which is essentially a surface. Occasional large radial vessels through a lamina connect the surface nets. Each lamina is divided into the three zones shown in Fig. 3. The first zone, which extends from the surface of the vascular network to about one third of the way across the lamina is composed of highly organized dense bone. The second zone, which extends the next one third of the distance is composed of poorly organized tissue. This zone is interrupted in the middle by a line that, under ordinary light microscopy, appears to be bright. This bright line is the boundary between the two blood supply networks bounding the lamina.

Cortical Haversian bone is also illustrated in Fig. 3 and its structure is further detailed in Fig. 4. It consists of quasi-cylindrically shaped elements called *osteons* or *Haversian systems.* The individual Haversian systems themselves are composed of concentric lamellae about 3 to 7 μm thick. These thin lamellae, in turn, are constructed from wrapped collagen fiberes impregnated at regularly spaced sites with hydroxyapatite and other mineral crystals about 20 to 40 nm long, cf. also [94].

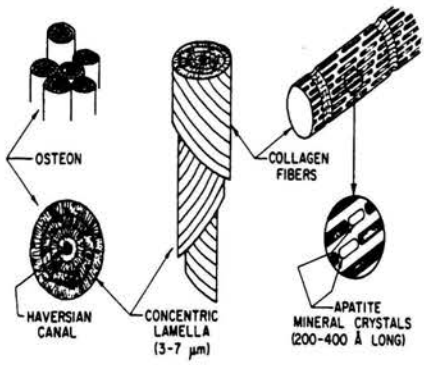

FIGURE 4. The detailed structure of an osteon, after Cowin [29].

Osteons are typically about 200 μm in diameter, the same thickness as the laminar bone, and about 10 to 20 mm long. The thickness is the same because the blood supply for the Haversian system is a central lumen containing a blood vessel, and thus every point in the Haversian system is no more than 100 μm from the blood supply, as was the case with laminar bone. Haversian bone is organized to accommodate small arteries, arterioles, capillaries and

venules of the microcirculating system. Haversian bone is never formed as a primary event, but forms as the result of the vascular invasion of bone. In young animals, woven bone is formed initially, the endosteal capillaries invade the avascular bone forming Haversian systems.

The osteons of Haversian bone and the laminae of laminar bone are basically just different geometric configurations of the same material. In both geometric configurations no point in the tissue is more than $100\,\mu$m away from the blood supply. The interfaces between the laminae in both Haversian and lamina bone contain an array of roughly ellipsoidal-shaped cavities called *lacunae* which contain bone cells, and from which extend numerous fine canals called the canaliculi. The thin layer between adjacent osteons is called the *cement line* and the three-dimensional region between osteons is filled with irregular pieces of lamellar bone. The canaliculi do not cross the cement line nor do they cross the bright lines between laminae in laminar bone.

Both Haversian and laminar bone occur simultaneously in the long human bones and in many animal bones including cattle. In the very young, the long bones are composed of woven bone with a few osteons, called *primary osteons*. With maturation the woven bone is coverted to laminar bone and, at maturity, there is a partial conversion to Haversian bone. According to [29], the convesion from laminar to Haversian bone is somewhat of a biological enigma. Haversian bone is known to have a less efficient local circulation system and to have a less mechanical strength compared to laminar bone and generally increases with age.

The composition of bone tissue is, very roughly, equal thirds by volume of minerals, water, and the extracellular collagenous matrix. If one tries to be more more precise about bone composition, then one must specify the species, the age, the sex, the specific bone in question, the type of bone tissue (cancellous or cortical), and whether the individual is experiencing a bone diseese or not, cf. [30].

Smith [71] proved the existence of several types of osteons composed of concentric lamellae. Ascenzi and Bonucci [11, 12, 13, 14] and Ascenzi *et al.* [15, 16] described the structure of bone consisting of three types of osteons with lamellae and fibers within these lamellae. Frasca [34] and Katz [49] described the fourth type of osteon, cf. also [5, 6, 7, 8, 9, 10, 15, 17, 18, 35]. The properies of single osteonic lamellae were studied in [10, 35, 65].

It seems that the first results pertaining to application of homogenization methods to finding macroscopic elastic moduli of compact bone are due to Aoubiza [3], Aoubiza *et al.* [4], Crolet [32] and Crolet *et al.* [33]. Telega *et al.* [36] claim that the macroscopic moduli can be derived provided that the

microscopic organization of bone in specified by the elasticity tensor

$$C_{ijkl}(x) = C_{ijkl}\left(\frac{x}{\varepsilon}, \frac{x}{\varepsilon^2}, \frac{x}{\varepsilon^3}\right), \tag{1.1}$$

where $\varepsilon > 0$ is a small parameter. There are thus three microscopic levels specified by $\frac{x}{\varepsilon}, \frac{x}{\varepsilon^2}, \frac{x}{\varepsilon^3}$. The determination of the macroscopic moduli C^h_{ijkl} means passing to zero with ϵ and is based on the so called *reiterated homogenization*. In [76] the authors proved that the effective moduli C^h_{ijkl} can be found by applying the Γ-convergence theory.

Typical examples of trabecular bones are shown in Figs. 5-7. These figures provide interesting visualization of human trabecular bone architecture

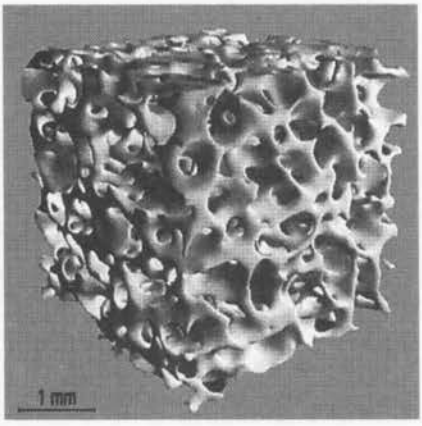

FIGURE 5. Micro-CT image of a trabecular bone specimen with rod-like architecture and a bone volume fraction of 26%, after [92].

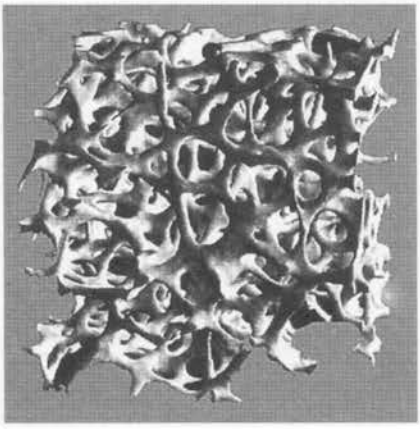

FIGURE 6. Trabecular bone with distinct rod-like columnar structure, after [57].

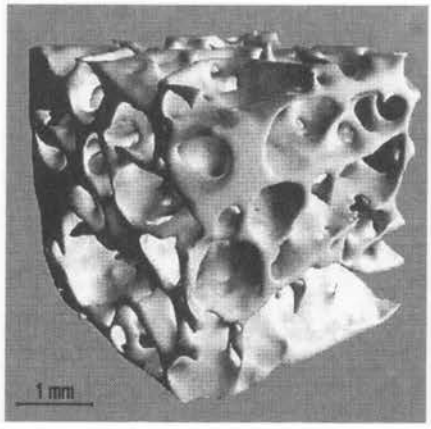

FIGURE 7. Micro-CT image of a trabecular bone specimen with plate-like architecture and a bone volume fraction of 26%, after [57].

obtained by micro-computed tomography, cf. Müller and Rüegsegger [57]; Ulrich *et al.*, [92]. According to Müller and Rüegsegger [57] specimens with diameters of a few millimeters to a maximum of 18 mm can be measured.

Figure 8 provides examples of idealized structures of cancellous bone. Different and combined architectures can also be envisaged.

The authors of the present synthetic paper published several articles on modeling of cancellous bone provided that it is treated as a cellular solid,

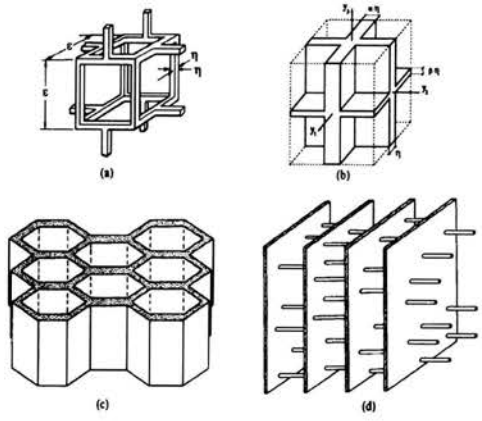

FIGURE 8. Models for the structure of cancellous bone: (a) the low-density equiaxed structure, (b) the higher-density equiaxed structure, (c) the stress-oriented prismatic structure and (d) the stress-oriented parallel plate structure, after [39].

starting from the paper [75]. Our results will be presented in this paper. In fact, cellular solids many be viewed as a specific case of *porous* materials. For various results on modeling cellular solids, including foams, the reader is referred to Roberts [67], Hohe and Becker [43], Shi and Tony [70], Overaker *et al.* [62], Warren and Kraynik [95], Roberts and Knackstedt [68], Vajjhala *et al.* [93], Ohno *et al.* [59, 60], Okumura *et al.* [61], Theocaris [79], Gibson *et al.* [40], Triantafillou *et al.* [91], Moore and Gibson [56].

Microstructure analyses of trabecular bone have followed the general approach used in the cellular plastics fields. McElhaney *et al.* [55] developed a porous block model of trabecular bone based on integration of spring stiffness loaded in parallel or in series. Using this model, they found good agreement between prediction of apparent stiffness and experimentally measured stiffness values in some internal layer of human skull. Pugh *et al.* [66] modeled the subchondral trabecular bone as a collection of structural plates and concluded that bending and buckling were major modes of deformation of the trabecular bone. Williams and Lewis [96] modeled the exact structure of a two-dimensional section of trabecular bone with plane strain finite elements to predict the apparent transversely isotropic elastic constants. Gibson [38] developed models of trabecular bone structure using analytical techniques for porous solids. He predicted the dependence of apparent stiffness on apparent density for different structural types of trabecular bones. Beaupré and Hayes [21] developed a three-dimensional spherical void model of trabecular bone and used finite element analyses to predict apparent stiffness and strength, as well the stress distribution within the trabecular. Hollister *et al.* [44, 45] applied the homogenization theory [25, 52, 69, 72] to an investigation of mechanical behavior of rod-like structures modeling the trabecular bone. By using the finite element method they evaluated the apparent, orthogonal Young's moduli and compared them with the experimental data obtained for proximal humerus, proximal tibia and distal femur, cf. also [42].

Bone may be viewed as a structurally hierarchical porous material. It is then possible to use the iterative homogenization [25] to derive the formulae for the macroscopic elastic moduli, cf. [3, 4, 32, 33]. Optimal design of structures often involves homogenization and relaxation methods [22, 24, 50, 52, 54]. Such an approach may be used to model bone microstructure via adaptive elasticity. Payten *et al.* [63] presented an optimization process that has, as its basis, an algorithm originally developed for predicting anatomical density distributions in natural human bones.

The microstructure of bone is such that at the macroscopic level its behaviour is anisotropic. To model bone anisotropy one can use Cowin's fabric tensor, see [30, 31, 46, 53] and the references cited therein. Jemioło and Telega [46] proved that compact bone is close to transverse isotropy whilst

trabecular bone is approximately orthotropic, cf. also [97] and the relevant papers in [31]. The approach employed in [46] exploits Cowin's fabric tensor. Detailed study of various approaches to fabric tensors in bone was performed by Jemioło and Telega [47]. In [97] the authors claim to use the homogenization method for finding the orthotropic elastic constants yet no precise formulation was unfortunately given.

A challenging problem in the estimation of bone elastic moduli is the influence of marrow. No satisfactory modeling of this problem seems to have been proposed so far. Kasra and Grynpas [48] proposed an idealized three-dimensional finite element model of a rod-like trabecular bone structure to study its static and dynamic response under compressive loading. Static analysis of the model predicted hydraulic stiffening of trabecular bone due to the presence of bone marrow. The predicted power equation relating the trabecular bone apparent elastic modulus to its apparent density was in good agreement with those of the reported experimental data. The influence of marrow was also studied by the first, second and fourth authors of the present paper, see Sec. 9, [77, 78, 87, 88, 90] and the paper by Arramon and Nauman in [31]

The aim of this paper is to present our macroscopic models of compact and cancellous bone by using the homogenization methods. General considerations pertaining to reiterated homogenization of linear elastic solid with three-scale microstructure are performed in Sec. 2. Section 3 is concerned with application of reiterated homogenization to finding effective macroscopic elastic moduli of compact bone with three structural levels. In Sec. 4 general homogenization procedure for the determination of elastic moduli of linear elastic porous material is sketched. The general approach is next used, in Secs. 5 and 6, to plate-like trabecular bone. Rod-like architecture is examined in Sec. 7. Honeycomb architecture is examined in Sec. 8. Section 9 is concerned with torsion of long bone where marrow is treated as a viscous material.

Homogenization problems considered in Secs. 5 and 7 involve two small parameters: ε and η. The first parameter is standard in the homogenization whilst the second parameter characterizes the thickness of plates or rods (trabeculae). To derive the formula for the elastic macroscopic moduli we first pass with ε to zero and next let η tend to zero. By properly choosing the geometry of the basic cell one can model anisotropic (orthotropic or transversely isotropic) behaviour of the cancellous bone at the macroscopic level. If $\alpha = \beta = 1$, at the macroscopic level the bone reveals the cubic symmetry, cf. formula (6.1). More complex architecture of trabecular bone requires more independent parameters. Such problem requires further studies.

2. Reiterated homogenization via Γ-convergence

In the next section the compact bone is modeled as the material with a hierarchical structure. Only three structural levels are considered. It is thus reasonable to assume that the elasticity tensor is given by

$$C^{\varepsilon}_{ijkl}(\mathbf{x}) = C_{ijkl}\left(\mathbf{x}, \frac{\mathbf{x}}{\varepsilon}, \frac{\mathbf{x}}{\varepsilon^2}, \frac{\mathbf{x}}{\varepsilon^3}\right) \tag{2.1}$$

where $C_{ijkl}(\mathbf{x}, \mathbf{y}_1, \mathbf{y}_2, \mathbf{y}_3)$ is $Y_1 \times Y_2 \times Y_3-$periodic in the second, third and fourth variables, and $\mathbf{y}_1 = \mathbf{x}/\varepsilon$, $\mathbf{y}_1 \in Y_1$ etc. Particularly, it may happen that $Y_1 = Y_2 = Y_3$, cf. Allaire and Briane [2]. We make the following assumptions, cf. Bensoussan *et al.* [25], Chapter 1, Sec. 8), Allaire and Briane [2]:

(i) $C^{\varepsilon}_{ijhl} \in L^{\infty}(\Omega)$,

(ii) there exists positive constants c_0 and c_1, $c_1 \geq c_0$ such that

$$\forall \mathbf{E} \in \mathbb{E}^3_s,\ c_0 E_{ij} E_{ij} \leq C_{ijkl}(\mathbf{x}, \mathbf{y}_1, \mathbf{y}_2, \mathbf{y}_3) E_{ij} E_{kl} \leq c_1 E_{ij} E_{ij}$$

almost everywhere in $\Omega \times Y_1 \times Y_2 \times Y_3$.

Here $\mathbb{E}^3_s$ denotes the space symmetric 3×3 matrices, and $\Omega \subset \mathbb{R}^3$ is a bounded, sufficiently regular domain representing the linear elastic body in its undeformed configuration. For fixed $\epsilon > 0$ the functional of the total potential energy is given by

$$J_{\varepsilon}(\mathbf{u}) = G_{\varepsilon}(\mathbf{u}) - L(\mathbf{u}), \tag{2.2}$$

where

$$G_{\varepsilon}(\mathbf{u}) = \frac{1}{2} \int_{\Omega} C^{\varepsilon}_{ijhl}(\mathbf{x}) e_{ij}(\mathbf{u}) e_{hl}(\mathbf{u}) d\mathbf{x}\,, \tag{2.3}$$

and $L(\mathbf{u})$ stands for the functional of the external loading. For instance, if the body is subjected to body forces $\mathbf{f} = (f_i)$ only, then

$$L(\mathbf{u}) = \int_{\Omega} f_i u_i d\mathbf{x}\,. \tag{2.4}$$

The strain tensor $\mathbf{e}(\mathbf{u})$ is linear:

$$\mathbf{e}_{ij}(\mathbf{u}) = u_{(i,j)} = \frac{1}{2}\left(\frac{\partial u_i}{\partial x_j} + \frac{\partial u_j}{\partial x_i}\right). \tag{2.5}$$

To perform homogenization when $\varepsilon \to 0$ the precise form o L is not required. It suffices to assume that L is a so called the perturbation functional, continuous in weak topology of $H^1(\Omega)^3 = [H^1(\Omega)]^3$.

Applying the Γ-convergence theory we conclude that the homogenized functional J_h is given by

$$J_h(\mathbf{u}) = \frac{1}{2}\int_{\Omega} C_{ijkl}(\mathbf{x})e_{ij}(\mathbf{u})e_{kl}(\mathbf{u})d\mathbf{x} - L(\mathbf{u}), \tag{2.6}$$

where the macroscopic elasticity tensor $\mathbf{C}^h$ is defined by the inductive homogenization formulae:

(a) $\mathbf{C}^{(3)} = \mathbf{C}(\mathbf{x}, \mathbf{y}_1, \mathbf{y}_2, \mathbf{y}_3)$,

(b) $\mathbf{C}^{(2)} = \mathbf{C}^2(\mathbf{x}, \mathbf{y}_1, \mathbf{y}_2)$ is obtained by periodic homogenization of $\mathbf{C}^{(3)}(\mathbf{x}, \mathbf{y}_1, \mathbf{y}_2, \frac{\mathbf{z}}{\varepsilon})$,

(c) $\mathbf{C}^{(1)} = \mathbf{C}^{(1)}(\mathbf{x}, \mathbf{y}_1)$ is obtained by periodic homogenization of $\mathbf{C}^2(\mathbf{x}, \mathbf{y}_1, \frac{\mathbf{z}}{\varepsilon})$,

(d) $\mathbf{C}^h(\mathbf{x}) = \mathbf{C}^0(\mathbf{x})$ is obtained by periodic homogenization of $\mathbf{C}^{(1)}(\mathbf{x}, \frac{\mathbf{z}}{\varepsilon})$.

More precisely, to derive the moduli $\mathbf{C}^{(2)}$, $\mathbf{C}^{(1)}$ and $\mathbf{C}^0$ we proceed as follows:

$$\begin{aligned} C^{(2)}_{mnpq}(\mathbf{x}, \mathbf{y}_1, \mathbf{y}_2) &= \frac{\partial W_2}{\partial E_{pq}\partial E_{mn}} \\ &= \frac{1}{|Y_3|}\int_{Y_3} C_{ijpq}(\mathbf{x}, \mathbf{y}_1, \mathbf{y}_2, \mathbf{y})(e^y_{ij}(\boldsymbol{\chi}^{(mn)}) + \delta_{im}\delta_{jn})d\mathbf{y} \end{aligned} \tag{2.7}$$

where

$$\begin{aligned} W_2(\mathbf{x}, \mathbf{y}_1, \mathbf{y}_2, \mathbf{E}) = \inf\left\{\tfrac{1}{|Y_3|}\right\}\int_{Y_3} C_{ijkl}(\mathbf{x}, \mathbf{y}_1, \mathbf{y}_2, \mathbf{y})(e^y_{ij}(\mathbf{v}) + E_{ij})\times \\ (e^y_{kl}(\mathbf{v}) + E_{kl})d\mathbf{y} \;\Big|\; \mathbf{v} \in \widetilde{H}^1_{per}(Y_1)^3,\ \ \mathbf{E} \in \mathbf{E}^3_s\,, \end{aligned} \tag{2.8}$$

and $\widetilde{H}^1_{per}(Y_3) = \{v \in H^1(Y_3) \mid$ v assumes equal values on the opposite sides of Y_3, $\langle v\rangle = 0\}$. Here

$$e^y_{ij}(\mathbf{v}) = \frac{1}{2}\left(\frac{\partial v_i}{\partial y_j} + \frac{\partial v_j}{\partial y_i}\right) \text{ and } \langle v\rangle_{Y_k} = \frac{1}{|Y_k|}\int_{Y_k} v d\mathbf{y},\ \ k = 1, 2, 3. \tag{2.9}$$

The function $\widetilde{\mathbf{v}}$, the solution of the minimization problem on the r.h.s. of (2.8) depends linearly on $\mathbf{E}$, i.e., $\widetilde{\mathbf{v}} = \boldsymbol{\chi}^{(mn)}E_{mn}$. The functions $\boldsymbol{\chi}^{(mn)} \in \widetilde{H}^1_{per}(Y_3)^3$ are solutions to the following local problem:

$$\int_{Y_3} C_{ijkl}(\mathbf{x}, \mathbf{y}_1, \mathbf{y}_2, \mathbf{y})(e^y_{ij}(\boldsymbol{\chi}^{(mn)}) + \delta_{im}\delta_{jn})e^y_{kl}(\mathbf{w})d\mathbf{z} = 0 \tag{2.10}$$

for any $\mathbf{w} \in \widetilde{H}^1_{per}(Y_3)^3$. Obviously, the functions $\boldsymbol{\chi}^{(mn)}(\mathbf{y}_3)$ depends also on $\mathbf{x}, \mathbf{y}_1$ and $\mathbf{y}_2$.

The moduli $C^{(1)}_{ijkl}(\mathbf{x}, \mathbf{y}_1)$ are found similarly. Finally, the macroscopic elastic moduli $C^h_{ijkl}(\mathbf{x}) = C^{(0)}_{ijkl}(\mathbf{x})$ are given by

$$C^h_{mnpq}(\mathbf{x}) = \frac{\partial W}{\partial E_{pq} \partial E_{mn}} = \frac{1}{|Y_1|} \int_{Y_1} C^{(1)}_{ijpq}(\mathbf{x}, \mathbf{y})(e^y_{ij}(\boldsymbol{\Phi}^{(mn)}) + \delta_{im}\delta_{jn}) e^y_{kl}(\mathbf{w}) d\mathbf{y} \tag{2.11}$$

where

$$\begin{aligned} W(\mathbf{x}, \mathbf{E}) = \inf \Big\{ \tfrac{1}{|Y_1|} \int_{Y_1} C^{(1)}_{ijkl}(\mathbf{x}, \mathbf{y})(e^y_{ij}(\boldsymbol{\xi}) + E_{ij}) \times \\ (e^y_{kl}(\boldsymbol{\xi}) + E_{kl}) d\mathbf{y} \mid \boldsymbol{\xi} \in \widetilde{H}^1_{per}(Y_1)^3 \Big\}, \quad \mathbf{E} \in \mathbf{E}^3_s \end{aligned} \tag{2.12}$$

and $\boldsymbol{\Phi}^{(mn)} \in \widetilde{H}^1_{per}(Y_1)^3$ is a solution to

$$\int_{Y_1} C^{(1)}_{ijkl}(\mathbf{x}, \mathbf{y})(e^y_{ij}(\boldsymbol{\Phi}^{(mn)}) + \delta_{im}\delta_{jn}) e^y_{kl}(\boldsymbol{\phi}) d\mathbf{y} = 0 \quad \forall \boldsymbol{\phi} \in \widetilde{H}^1_{per}(Y_1)^3 \tag{2.13}$$

Remark 1. More general scaling than that described by ε, ε^2 and ε^3 is possible. The elasticity tensor $\mathbf{C}^\varepsilon$ can be given by, cf. Allaire and Briane [2]

$$C^\varepsilon_{ijkl}(\mathbf{x}) = C_{ijkl}\left(\mathbf{x}, \frac{\mathbf{x}}{\varepsilon_1}, \frac{\mathbf{x}}{\varepsilon_2}, \frac{\mathbf{x}}{\varepsilon_3}\right), \tag{2.14}$$

provided that

$$\lim_{\varepsilon \to 0} \frac{\varepsilon_3}{\varepsilon_2} = 0, \quad \lim_{\varepsilon \to 0} \frac{\varepsilon_2}{\varepsilon_1} = 0, \quad \varepsilon_k = \varepsilon_k(\varepsilon). \tag{2.15}$$

This means that each scale can be distinguished from the others (separation of scales), i.e., they are not of the same order of magnitude. In (2.1) we obviously have

$$\varepsilon_k = \varepsilon^k, \quad k = 1, 2, 3. \tag{2.16}$$

Remark 2. The reiterated homogenization procedure can be extended to perforated domains described as follows. For each $k = 1, 2, 3$, the basic cell Y_k is divided into a material part Y^*_k and the whole T_k. The case where T_k is empty is not precluded. Now the integrals in (2.3) and (2.4) are calculated over the domain Ω_ε, being the multiscale perforated domain, cf. Allaire ans Briane [2]. We observe that peforated materials are more appropriate as models of bone tissue.

To derive the homogenized moduli we proceed similarly as previously, except that now the integrals over Y_k, $k = (1,2,3)$ are to be replaced by integrals over Y_k^* and the spaces $\widetilde{H}^1_{per}(Y_k^*)$ replace the spaces $\widetilde{H}^1_{per}(Y_k)$. Moreover, if L is given by

$$L_\varepsilon(\mathbf{u}) = \int_{\Omega_\varepsilon} f_i u_i d\mathbf{x} + L_1(\mathbf{u}), \tag{2.17}$$

then

$$L_h(\mathbf{u}) = \int_{\Omega_\varepsilon} \Theta f_i u_i d\mathbf{x} + L_1(\mathbf{u}) \tag{2.18}$$

where $\Theta = \Theta_1\Theta_2\Theta_3$ is the overall volume fraction of material, $\Theta_k = |Y_k^*|$.

3. Application of reiterated homogenization to the determination of effective elastic moduli of compact bone

As we already know, compact bone is characterized by many structural levels. Here we are going to consider three of them, most important from the point of you of finding the macroscopic elastic moduli. We follow the thesis [3] and [4, 32, 34, 36].

At the *lowest* level, the lamellar structure is considered: collagen fibres are embedded in hydroxyapatite crystals. In a single lamella, all the collagen fibres have the same orientation but the orientation of these fibres can differ between two adjacent lamellae.

The *second* level corresponds to the structural definition of a single osteon and of a part of the interstitial system, an osteon being a set of concentric lamellae, which surround the Haversian canal.

At the *highest* level, a representative volume of compact bone is examined. This volume consists of sufficiently large number of osteons embedded in the interstitial system. The osteons are packed tightly together, mutually parallel and oriented in the direction of the long axis of the bone.

3.1. Modeling of the lamellar structure

The simulation of the characteristics of a single lamella is performed in two steps. First, a lamella is divided into a finite number of identical cylindrical sectors, cf. Fig.9. By knowing the elasticity tensor of one sector, the elasticity tensor of any other sector can obviously be calculated. It suffices to perform a rotation. Secondly, the cylindrical sector is geometrically approximated by a parallelepiped sector and, through a change of axis, the directions of fibres are assumed to be parallel to one side of this cubic sector. In the

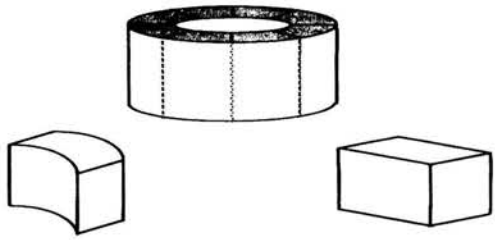

FIGURE 9. Decomposition of a lamella and approximation of a sector, after Crolet *et al.* [33].

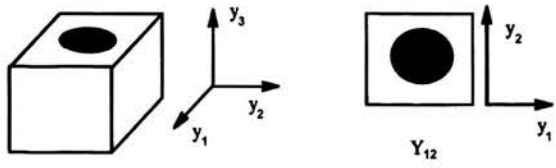

FIGURE 10. Basic cell for the homogenization in a sector, after Crolet *et al.* [33].

case of the cubic sector (fibrous unidirectional composite), the basic cell Y_3 is chosen to be a collagen fiber and a hydroxyapatite matrix, see Fig. 10.

In this case the homogenization is two- dimensional. It means that the homogenized coefficients $C^{(2)}_{ijkl}$ are calculated according to the formula (2.7). To solve this two- dimensional homogenization problem one can use a FEM. In this manner the homogenization moduli of a lamella sector are obtained. The direction of fibres was assumed to be parallel to the longitudinal axis of the lamella. In more general case, where the fibres are oriented with respect to the longitudinal axis one can use the transformation formula, cf. Fig. 11.

Crolet *at al.* [33] and Aoubiza *at al.* [4] assumed that the collagen and hydroapatite are homogeneous, isotropic and perfectly bonded. Such an idealization is enforced by available experimental data.

3.2. Methods of calculation

In essence, our procedure is divided into four steps.

Step 1. *Calculation of material constants for osteon and interstitial system.*

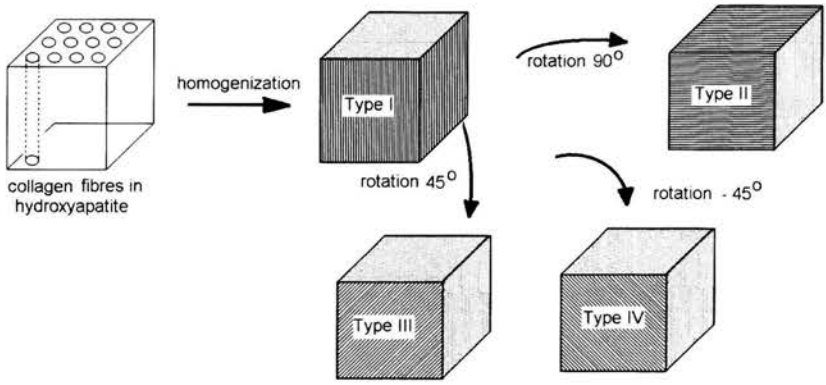

FIGURE 11. Various orientation of collagen fibers.

To obtain the effective elastic constants for material of osteons lamella of type I we use the Christensen formulae [26]. These formulae give the effective properties of mixture of circular fibers in isotropic matrix. The fibers are made of collagen and hydroxyapatite matrix.
The material constants for collagen are given by [29]:

$$\rho_c = 1.40, \quad E_c = E_1 = 1.2, \quad \nu_c = \nu_1 = 0.35\,.$$

The material constants for the hydroxyapatite are assumed to be given by:

$$\rho_h = 3, \quad E_h = E_2 = 114, \quad \nu_h = \nu_2 = 0.27\,.$$

If k denotes the mineral content then the volume fraction ϕ of collagen is derived from the formula

$$\phi = \frac{(1-k)\,\rho_h \rho_c}{k\,\rho_c\,[k\,\rho_c + (1-k)\,\rho_h]}. \tag{3.1}$$

For the mineral content 58% (osteon) and 63% (interstitial system), we have $\phi = 0.608$ and $\phi = 0.557$, respectively. The elastic effective constants for lamella of type I are calculated for both cases.

Type II is obtained from the material constants tensors for type I by rotation through the angle 90° with respect to the Ox axis.

Type III is obtained from material constants tensors for type I by rotation angle 45° with respect to Ox axis.

Type IV is obtained by rotation angle $-45°$ with respect to Ox axis.

The architecture VI is calculated as for layered structure by homogenization formulae for anisotropic components of types I, II , III and IV with the volume fraction 0.25. The transversely isotropic properties of material of osteon and interstitial system are calculated by integration over the direction of lamination.

First, material properties of lamella of type I are calculated. Next lamellae of types II, III and IV are investigated by appropriate rotations of fibers in the matrix.

Step 2. *Calculation of material constants for osteon and interstitial system.*

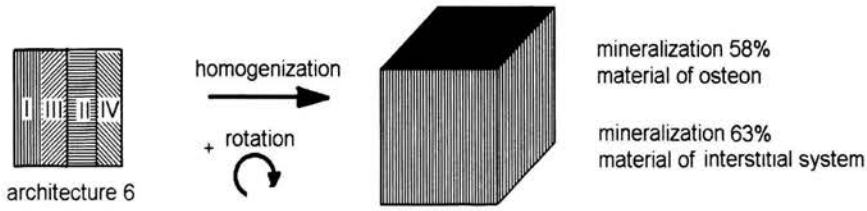

FIGURE 12. Specific case of lamellae arrangement.

Each osteon consists of lamellae having the same thickness and two adjacent lamellae are perfectly bonded, cf. Fig. 12. The results from the previous level are used as the data for the second level. This simulation was also used to obtain the moduli of the interstitial system. The latter is assumed to be a fragment of "old" osteons. In this case, the degree mineralization is assumed to be more elevated.

Crolet *et al.* [33] studied six architectures of compact bones:

- architecture No 1: one type of osteons (type I);
- architecture No 2: one type of osteons (type II);
- architecture No 3: one type of osteons (type IV);
- architecture No 4: two types of osteons (I and II) in the same proportion;
- architecture No 5: three types of osteons (types I, II and III) in the following proportions: 25, 25 and 50%;
- architecture No 6: four types of osteons (types I-IV) in the proportions: 25, 25, 25 and 25%.

Obviously, one can also envisaged different architectures. In what follows the architecture 6 is considered. Secondly, the architectures VI and VII are calculated as multilayered structures by homogenization formulae for anisotropic components. Finally, the transversely isotropic properties of material of osteon and interstitial system are calculated by integration over direction of lamination with diffrent mineral content (less for osteon material).

Step 3. *The method of calculation of effective material constants of osteon with Haversian canal.*

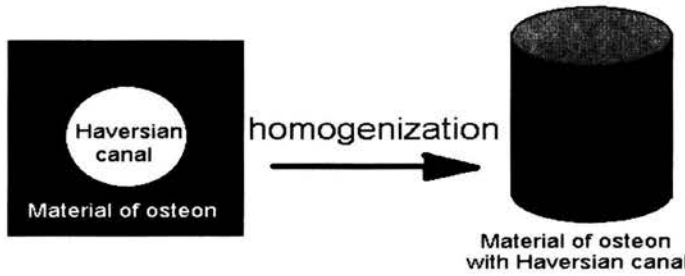

FIGURE 13. Osteon with Haversian canal.

At first our FEM method was applied to calculate the effective properties of osteon with fixed volume fraction of Haversian canal (modeled by a cavity) with square section. Next, by integration over rotation angle the transversely isotropic moduli of osteon material with Haversian canal are calculated. This procedure is repeated for different volume fraction of Haversian canal: 0.133, 0.15, 0.2, 0.25 and 0.3.

Step 4. *The method of calculation of effective material constants of compact bone.*

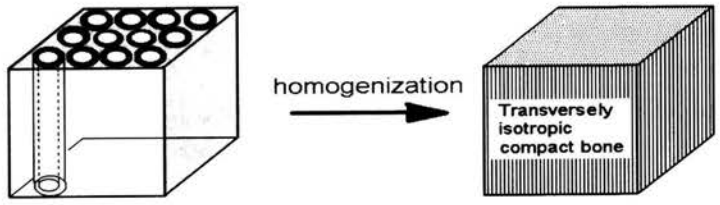

FIGURE 14. The final step of homogenization.

Effective properties of compact bone are calculated similarly to Step 2. At first our FEM method was applied to calculate the effective properties of bone with fixed volume fracture of osteon equal to 75% for different volume fractions of Haversian canal in osteons with square section. Secondly, by integration over rotation angle the transversely isotropic moduli of compact bone material are obtained.

3.3. Results

Technical constants calculated according to the outlined procedure are given in Table 1 in rows 1-5, for the following volume fractions of Haversian canal: 0.133, 0.15, 0.2, 0.25 and 0.3, respectively. In row 6 the results due to Crolet *et al.* [33] given, whilst in row 7 the experimental data obtained on dry bone are provided. In Table 1, A6-1 denotes the architecture no. 6 with the volume fraction of Haversian canal 0.133, and similarly for A6-2,...,A6-5

TABLE 1. Comparison of technical moduli.

	E_1	E_3	G_{13}	G_{12}	ν_{12}	ν_{13}	ν_{31}
A6-1	24.33	31.12	10.69	9.95	0,22	0.19	0,24
A6-2	3.60	30.71	10.45	9.63	0.23	0.19	0.24
A6-3	21.48	29.46	9.75	8.71	0.24	0.18	0.24
A6-4	19.50	28.21	9.08	7.86	0.25	0.17	0.24
A6-5	17.66	26.98	8.43	7.07	0.26	0.16	0.24
A6- Crolet *et al.* [33]	17.87	33.3	6.7	5.48	0.31	0.13	0,23
Yoon and Katz [98]	18.80	27.40	8.71	7.17	0.31	0.19	0.28

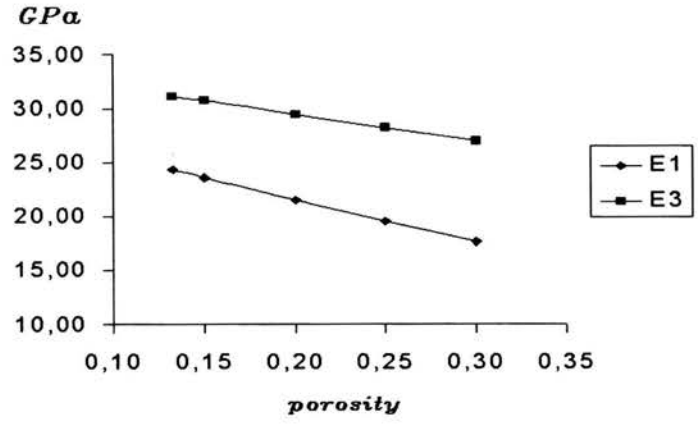

FIGURE 15. Young moduli versus porosity.

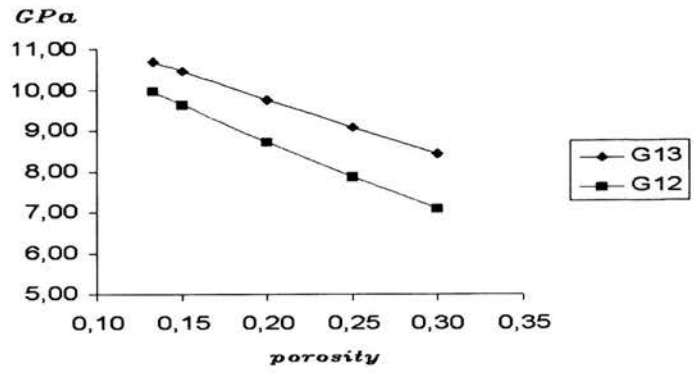

FIGURE 16. Shear moduli as function of porosity.

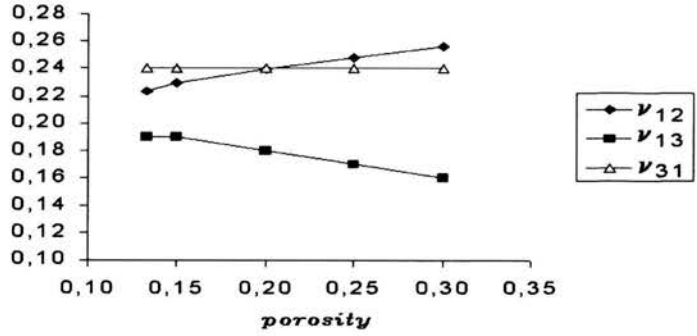

FIGURE 17. Poisson's ratios versus porosity.

with the volume fraction 0.15, 0.2, 0.25 and 0.3, respectively. The depedence of technical constants on porosity is depicted in Figs. 15-17.

4. Homogenization of porous linear elastic materials

Let Ω denote a bounded open subset of $\mathbb{R}^3$. As usual, by Y we denote the basic cell, cf. [25, 52, 69, 72]. The part of Y occupied by the material is denoted by Y^*. It is assumed that the hole T in Y does not intersect the boundary ∂Y, cf. [27, 52], though this assumption may be weakened. By Ω_ε^* we denote the part of Ω occupied by the material. Here $\varepsilon > 0$ is a small parameter. Let us consider the following boundary value problem of linear

elasticity [27, 28]

$$\frac{\partial}{\partial x_j}\left(C_{ijkl}\left(\frac{\mathbf{x}}{\varepsilon}\right)\frac{\partial u_k^\varepsilon}{\partial x_l}\right)+f_i=0 \quad \text{in } \Omega_\varepsilon^*,$$

$$u_k^\varepsilon=0 \quad \text{on} \quad \partial\Omega, \tag{4.1}$$

$$C_{ijkl}\left(\frac{\mathbf{x}}{\varepsilon}\right)\frac{\partial u_k^\varepsilon}{\partial x_l}n_j=0 \qquad \text{on } \partial\Omega_\varepsilon^*\backslash\partial\Omega,$$

where $\mathbf{n}=(n_j)$ is the unit vector normal to $\partial\Omega_\varepsilon^*\backslash\partial\Omega$. We make the following assumptions:

(i) $f_i\in L^2(\Omega)$,

(ii) $C_{ijkl}\in L^\infty(Y^*)$, $C_{ijkl}=C_{klij}=C_{jikl}$ $i,j,k,l=1,2,3$.

(iii) There exist a positive constant c_0 such that for almost every $\mathbf{y}\in Y$: $C_{ijkl}(\mathbf{y})e_{ij}e_{kl}\geq C_0e_{ij}e_{ij}$ for any $\mathbf{e}=(e_{ij})$, $e_{ij}=e_{ji}$;

(iv) The material coefficients $C_{ijkl}(\mathbf{y})$ are Y-periodic.

The passage with ε to zero is now standard. Let us recall the related basic results which will next be exploited in Sec. 5, where we will let a parameter η introduced below to tend to zero. Under these assumptions, there exists an extension $P_\varepsilon\mathbf{u}^\varepsilon\in\left[H_0^1(\Omega)\right]^3$ of $\mathbf{u}^\varepsilon$ such that, cf. [28],

$$P_\varepsilon\mathbf{u}^\varepsilon\rightharpoonup\mathbf{u} \quad \text{in } \left[H_0^1(\Omega)\right]^3 \text{ weakly},$$

with $\mathbf{u}=(u_k)$ being the solution to:

$$C_{ijkl}^h\frac{\partial^2u_k}{\partial x_j\partial x_l}+\frac{|Y^*|}{|Y|}f_i=0 \quad \text{in } \Omega, \qquad \mathbf{u}=\mathbf{0}, \quad \text{on } \partial\Omega. \tag{4.2}$$

We recall that $|Y|=vol\ Y$.
The homogenized coefficient C_{ijkl}^h are given by

$$C_{ijmn}^h=<C_{ijmn}>+<C_{ijpq}\frac{\partial\chi_p^{(mn)}}{\partial y_q}>, \tag{4.3}$$

where

$$<\cdot>=\frac{1}{|Y|}\int_{Y^*}(\cdot)d\mathbf{y}.$$

The Y-periodic functions $\chi_p^{(mn)}$ are solutions to the local problem

$$\frac{\partial}{\partial y_i}\left(C_{ijmn}\frac{\partial}{\partial y_n}\left(\chi_m^{(pq)}+\delta_{mp}y_q\right)\right)=0 \quad \text{in } Y^*, \tag{4.4}$$

$$C_{ijmn}\frac{\partial}{\partial y_n}\left(\chi_m^{(pq)}+\delta_{mp}y_q\right)N_i=0 \quad \text{on } \partial T. \tag{4.5}$$

Here $\mathbf{N}$ stands for the inner unit vector normal to ∂T. Written in the weak form, this problem is expressed by

$$\int_{Y^*} C_{ijmn}\frac{\partial\chi_m^{(pq)}}{\partial y_n}\frac{\partial\Psi_j}{\partial y_i}\,d\mathbf{y}=-\int_{Y^*} C_{ijpq}\frac{\partial\Psi_j}{\partial y_i}\,d\mathbf{y}, \qquad \forall\ \Psi_j\in H_{per}(Y^*), \tag{4.6}$$

where

$$H_{per}(Y^*)=\left\{v\in H^1(Y^*)\mid v \text{ is } Y-\text{periodic}\right\}.$$

For $\Psi_j=\chi_j^{(pq)}$ we get

$$\int_{Y^*} C_{ijmn}\frac{\partial\chi_m^{(pq)}}{\partial y_n}\frac{\partial\chi_j^{(pq)}}{\partial y_i}\,d\mathbf{y}=-\int_{Y^*} C_{ijpq}\frac{\partial\chi_j^{(pq)}}{\partial y_i}\,d\mathbf{y}. \tag{4.7}$$

5. Plate-like structure

In this section we shall derive the macroscopic moduli for a cellular solid with plate-like architecture. The first step of homogenization has been performed in the previous section. The plates are characterized by a small parameter $\eta>0$. One can easily envisage more complex plate-like architectures with plates (trabeculae) not necessarily orthogonal and of constant thickness. Plates may also be perforated. More complex architecture would require more independent geometrical parameters (or functions). Then, however, one has to resort to numerical methods to find the effective moduli, cf. Kowalczyk [51]. In the case considered the second step of homogenization consists in passing with η to zero. Let now the basic cell Y be given by

$$Y=[-\frac{1}{2},\frac{1}{2})\times[-\frac{1}{2},\frac{1}{2})\times[-\frac{1}{2},\frac{1}{2}). \tag{5.1}$$

Due to periodicity, the homogenized coefficients do not depend on the basic cell and consequently, one may take a translated cell of the basic one. Consequently we take a translated cell represented in Fig. 18.

We observe that the thicknesses of three orthogonal plates are not necessarily equal, thus allowing for a macroscopically orthotropic response of the trabecular bone. Let us introduce the following notation:

$$Y_1=\left\{\mathbf{y}\in Y, |y_1|\le\frac{\eta}{2}\right\},$$

$$Y_2=\left\{\mathbf{y}\in Y, |y_2|\le\alpha\frac{\eta}{2}\right\},$$

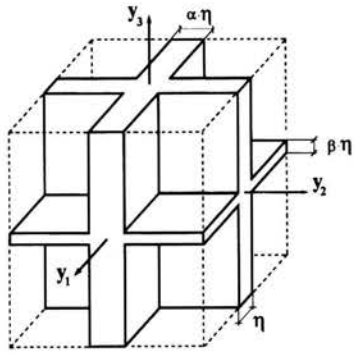

FIGURE 18. Translated basic cell.

$$
\begin{aligned}
Y_3 &= \left\{\mathbf{y} \in Y, |y_3| \le \beta\frac{\eta}{2}\right\},\\
Y_{12} &= \left\{\mathbf{y} \in Y, |y_1| \le \frac{\eta}{2} \text{ and } |y_2| \le \alpha\frac{\eta}{2}\right\},\\
Y_{23} &= \left\{y \in Y, |y_2| \le \alpha\frac{\eta}{2} \text{ and } |y_3| \le \beta\frac{\eta}{2}\right\},\\
Y_{13} &= \left\{\mathbf{y} \in Y, |y_1| \le \frac{\eta}{2} \text{ and } |y_3| \le \beta\frac{\eta}{2}\right\},\\
Y_{123} &= \left\{\mathbf{y} \in Y, |y_1| \le \frac{\eta}{2} \text{ and } |y_2| \le \alpha\frac{\eta}{2} \text{ and } |y_3| \le \beta\frac{\eta}{2}\right\},\\
Y_\eta^* &= \left\{\mathbf{y} \in Y, |y_1| \le \frac{\eta}{2} \text{ or } |y_2| \le \alpha\frac{\eta}{2} \text{ or } |y_3| \le \beta\frac{\eta}{2}\right\}.
\end{aligned}
\tag{5.2}
$$

Since $|Y_\eta^*| = (1+\alpha+\beta)\,\eta - (\alpha+\beta+\alpha\,\beta)\,\eta^2 + \alpha\,\beta\,\eta^3$, we get the following estimate:

$$
||\mathbf{e}^y(\boldsymbol{\chi}^{(pq)})||_{L^2(Y_\eta^*)} \le c\,\eta^{1/2},\ p,q = 1,2,3. \tag{5.3}
$$

Obviously $\boldsymbol{\chi}^{(pq)}$ depend on α, β and η. The constant c is independent of η and

$$
e^y(\mathbf{w}) = \frac{1}{2}\left(\frac{\partial w_i}{\partial y_j} + \frac{\partial w_j}{\partial y_i}\right).
$$

Using this estimate in (4.3) we conclude that

$$
\eta^{-1} C^h_{ijmn} \to C^*_{ijmn}
$$

(after extraction of a subsequence, if necessary) We can pass to the limit as $\eta \to 0$ in the homogenized equation (4.2), whose solution is denoted by $\mathbf{u}^\eta$. We have

$$
u^\eta_k \rightharpoonup u^*_k \quad \text{in } H^1_0(\Omega) \text{ weakly},
$$

where $\mathbf{u}^*$ is the solution to:

$$C^*_{ijkn}\frac{\partial^2 u^*_k}{\partial x_j \partial x_n} + (1+\alpha+\beta)\, f_i = 0 \quad \text{in } \Omega, \qquad \mathbf{u}^* = 0 \quad \text{on } \partial\Omega. \tag{5.4}$$

We observe that now $|Y| = 1$. After lengthy calculations we finally obtain:

$$\begin{aligned} C^*_{ijmn} &= (1+\alpha+\beta)\, C_{ijmn} - C_{ijp1}\left(\mathbf{C}_1^{-1}\right)_{pq} C_{1qmn} \\ &\quad - \alpha\, C_{ijp2}\left(\mathbf{C}_2^{-1}\right)_{pq} C_{2qmn} - \beta\, C_{ijp3}\left(\mathbf{C}_3^{-1}\right)_{pq} C_{3qmn}. \end{aligned} \tag{5.5}$$

For the proof the reader is referred to Gałka *et al.* [37]. Here $\left(\mathbf{C}_2^{-1}\right)_{mj}$ and $\left(\mathbf{C}_3^{-1}\right)_{mj}$ are the components of the matrices inverse to (C_{2mj2}) and (C_{3mj3}) respectively.

If we take a more general basic cell:

$$Y = [-\frac{1}{2}, \frac{1}{2}) \times [-\frac{A}{2}, \frac{A}{2}) \times [-\frac{B}{2}, \frac{B}{2})$$

then we obtain the following formula:

$$\begin{aligned} C^*_{ijmn} &= (1+\frac{\alpha}{A}+\frac{\beta}{B})\, C_{ijmn} - C_{ijp1}\left(\mathbf{C}_1^{-1}\right)_{pq} C_{1qmn} \\ &\quad - \frac{\alpha}{A}\, C_{ijp2}\left(\mathbf{C}_2^{-1}\right)_{pq} C_{2qmn} - \frac{\beta}{B}\, C_{ijp3}\left(\mathbf{C}_3^{-1}\right)_{pq} C_{3qmn}. \end{aligned} \tag{5.6}$$

Remark 3. To make the plate-like model of cancellous bone more realistic, the plates constituting the basic cell should have holes. Then the plates would be weaker and parameters characterizing the holes would intervene in the formula for the elasticity matrix $\mathbf{C}^*$. More precisely, the elastic potential with the elastic moduli (5.6) represents then an upper bound for plate-like cellular material with perforated plate-like trabeculae.

6. Specific case: trabecular plates made of a homogeneous and isotropic material

Let the plate trabeculae be isotropic and homogeneous; then

$$C_{ijmn} = \mu\,(\delta_{mj}\delta_{ni} + \delta_{mi}\delta_{nj}) + \lambda\delta_{ij}\delta_{mn}.$$

From (5.5) we obtain the following form of the elasticity matrix:

$$\mathbf{C}^* = \begin{bmatrix} \frac{4\mu(\alpha+\beta)(\lambda+\mu)}{2\mu+\lambda} & \frac{2\beta\lambda\mu}{2\mu+\lambda} & \frac{2\alpha\lambda\mu}{2\mu+\lambda} & 0 & 0 & 0 \\ \frac{2\beta\lambda\mu}{2\mu+\lambda} & \frac{4\mu(1+\beta)(\lambda+\mu)}{2\mu+\lambda} & \frac{2\lambda\mu}{2\mu+\lambda} & 0 & 0 & 0 \\ \frac{2\alpha\lambda\mu}{2\mu+\lambda} & \frac{2\lambda\mu}{2\mu+\lambda} & \frac{4\mu(1+\alpha)(\lambda+\mu)}{2\mu+\lambda} & 0 & 0 & 0 \\ 0 & 0 & 0 & 2\mu & 0 & 0 \\ 0 & 0 & 0 & 0 & 2\alpha\mu & 0 \\ 0 & 0 & 0 & 0 & 0 & 2\beta\mu \end{bmatrix}.$$

Obviously, here Voigt's notation has been used, cf. [58].

Having in mind Fig. 18, the *physical* effective elasticity tensor, now denoted by $\mathbf{C}^{\text{eff}}$, is given by

$$\mathbf{C}^{\text{eff}} = \frac{\phi}{1+\alpha+\beta}\,\mathbf{C}^{*}, \tag{6.1}$$

where ϕ is the volume fraction. In the case of $\mathbf{C}^{*}$ given by Eq. (5.6) we have

$$\mathbf{C}^{\text{eff}} = \frac{\phi AB}{AB + B\alpha + A\beta}\,\mathbf{C}^{*}.$$

By $\mathbf{A}$ we denote the matrix inverse to $(\mathbf{C}^{\text{eff}})$, i.e. $\mathbf{A} = \left(\mathbf{C}^{\text{eff}}\right)^{-1}$. Then the technical elasticity constants are, cf. [46], [58],

$$E_1 = \frac{1}{A_{11}},\quad E_2 = \frac{1}{A_{22}},\quad E_3 = \frac{1}{A_{33}}; \tag{6.2}$$

$$G_{12} = \frac{1}{2\,A_{66}},\quad G_{13} = \frac{1}{2\,A_{55}},\quad G_{23} = \frac{1}{2\,A_{44}}; \tag{6.3}$$

$$\begin{aligned} &\nu_{12} = -\frac{A_{12}}{A_{22}},\quad \nu_{21} = -\frac{A_{12}}{A_{11}},\quad \nu_{13} = -\frac{A_{13}}{A_{33}},\\ &\nu_{31} = -\frac{A_{12}}{A_{11}},\quad \nu_{23} = -\frac{A_{23}}{A_{33}},\quad \nu_{32} = -\frac{A_{23}}{A_{22}}. \end{aligned} \tag{6.4}$$

Let us pass now to the presentation of specific cases, which show the usefulness of the formulae (6.1) for the determination of macroscopic elastic moduli of trabecular bone with plate-like architecture. These particular cases are presented in the form of Tables 2, 3 and 4 and Figs. 19-21 below.

TABLE 2. Technical constants: cortical bone.

Techn. const. (average)	human cortical bone	from (6.2)-(6.4) $E = 114$ GPa, $\nu = 0.27$
E_1	11.7 (1.6) GPa	11.7 GPa
E_2	13.2 (1.8) GPa	14.4 GPa
E_3	19.8 (2.4) GPa	19.8 GPa
G_{12}	4.53 (0.37) GPa	1.1 GPa
G_{13}	5.61 (0.4) GPa	3.27 GPa
G_{23}	6.23 (0.48) GPa	4.36 GPa
ν_{12}	0.375 (0.095)	0.04
ν_{21}	0.416 (0.118)	0.03
ν_{23}	0.237 (0.083)	0.21
ν_{32}	0.346 (0.096)	0.15
ν_{13}	0.374 (0.108)	0.19
ν_{31}	0.234 (0.088)	0.11

The third column of Table 2 provides technical constants calculated by using formulae (6.2)-(6.4). The following data, corresponding to the hydroxyapatite, cf. [30, 31, 33], are assumed:

$$E = 114\,\text{GPa}, \quad \nu = 0.27.$$

Then the Lamé coefficients are given by $\lambda = 52.69\,\text{GPa}$, $\mu = 44.88\,\text{GPa}$ The calculations have been performed for

$$\alpha = \frac{3}{4}, \quad \beta = \frac{1}{4}, \quad \phi = \frac{1}{5}.$$

The second column in Table 2 is taken from Table 1 in [46].
Two further specific cases are summarized in the third and fourth column of Table 3. To calculate the moduli given in the third column of this table it was assumed that

$$\lambda = 52.69\,\text{GPa}, \ \mu = 44.88\,\text{GPa}, \ \alpha = \frac{56}{67}, \ \beta = \frac{73}{134}, \ \phi = 0.007.$$

Similarly, the moduli contained in the fourth column were calculated for the following data:

$$\lambda = 17.28\,\text{GPa}, \ \mu = 7.41\,\text{GPa}, \ \alpha = \frac{56}{67}, \ \beta = \frac{73}{134}, \ \phi = 0.043.$$

The second column of Table 3 is taken from Table 1 in [46]. According to Table 9 in [30], $E = 20\,\text{GPa}$ estimates the value of the elastic modulus of the wet human trabecula.

We observe that the second column of Table 1 in [46] (or the second column in our Table 2) presents technical constants for specimens of human femoral cortical bone, where the 1-direction is radial, the 2-direction

TABLE 3. Technical constants: cancellous bone.

	human cancellous bone (proximal tibia)	$E = 114\,\text{GPa}$, $\nu = 0.27$	$E = 20\,\text{GPa}$, $\nu = 0.35$
E_1	237 (63) MPa	496 MPa	545 MPa
E_2	309 (93) MPa	552 MPa	604 MPa
E_3	823 (337) MPa	649 MPa	706 MPa
G_{12}	73 (0.37) MPa	73 MPa	73 MPa
G_{13}	112 (0.4) MPa	112 MPa	112 MPa
G_{23}	134 (0.48) MPa	134 MPa	134 MPa
ν_{12}	0.169 (0.304)	0.08	0.1
ν_{21}	0.209 (0.209)	0.07	0.09
ν_{23}	0.063 (0.217)	0.15	0.18
ν_{32}	0.245 (0.626)	0.11	0.14
ν_{13}	0.423 (0.356)	0.16	0.2
ν_{31}	0.145 (0.123)	0.14	0.17

is circumferential and the 3-direction is longitudinal. The second column of Table 3 presents average technical constants for 9 specimens of human cancellous bone from the proximal tibia, where the 1-direction is anterior-posterior, the 2-direction is medial and 3-direction is logitudinal. In Tables 2 and 3 the numbers in parantheses stand for standard deviations. The second column of Table 3 implies a possibility of appearance of negative values of Poisson's ratios. The plate-like architecture studied in the present paper precludes such possibility. Examples of cellular solids with negative Poisson's ratio are given in [23, 31]. Thus a natural question arises: can trabecular bone, at a certain stage of human or animal life, behave like a cellular solid with negative Poisson's ratio? From the theoretical point of view such possibility is obviously possible. The decisive answer, however, is to be expected from experimentalists. Negative Poison's ratio is in fact nothing surprizing, since it is allowed by the positiveness of the elastic energy of anisotropic materials. We observe that according to Table 9 in [30], the value of E equal to 1.17 GPa characterizes individual bovine trabeculae. This result was obtained by Christensen (cf. [30]) using statistical data analysis. In Table 9 in [30] one also finds the following values of E [GPa] for individual trabeculae:

$E = 10.90 \pm 1.6$ – wet bovine femur, ultrasonic test method,

$E = 12.70 \pm 2$ – wet human femur, ultrasonic test method,

$E = 8.69 \pm 3.17$ – dry human distal femur, buckling test method,

$E = 5.3 \pm 2.6$ – dried human femur, experimental test method with finite element method.

TABLE 4. Technical constants from (6.2)-(6.4)

	$E = 1$ GPa $\nu = 0.35$ $\alpha = 0.836$ $\beta = 0.545$ v = 0.1	$E = 1$ GPa $\nu = 0.35$ $\alpha = 0.836$ $\beta = 0.545$ v = 0.3	$E = 5$ GPa $\nu = 0.3$ $\alpha = 0.9$ $\beta = 0.2$ v = 0.2	$E = 10$ GPa $\nu = 0.35$ $\alpha = 0.9$ $\beta = 0.2$ v = 0,2
E_1	0.0633 MPa	0.19 MPa	0.545 MPa	1.14 MPa
E_2	0.701 MPa	0.21 MPa	0.603 MPa	1.23 MPa
E_3	0.819 MPa	0.246 MPa	0.924 MPa	1.87 MPa
G_{23}	0.0156 MPa	0.0467 MPa	0.183 MPa	0.353 MPa
G_{13}	0.013 MPa	0.039 MPa	0.165 MPa	0.317 MPa
G_{12}	0.008 MPa	0.0254 MPa	0.0366 MPa	0.0705 MPa
ν_{23}	0.204	0.204	0.238	0.276
ν_{32}	0.175	0.175	0.156	0.182
ν_{12}	0.101	0.101	0.0164	0.0114
ν_{21}	0.0913	0.0913	0.0151	0.105
ν_{13}	0.184	0.184	0.232	0.269
ν_{31}	0.142	0.142	0.14	0.164

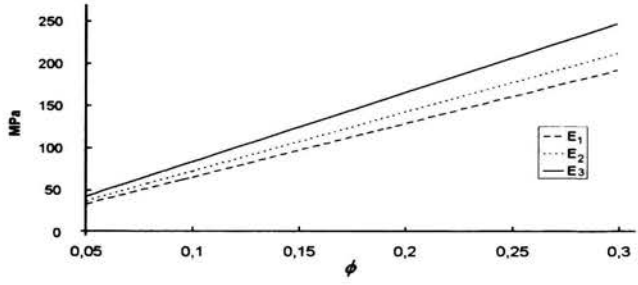

FIGURE 19. Young's moduli in the three orthotropic principal directions versus bone volume fractions; $\alpha = 56/67$, $\beta = 73/134$; isotropic trabeculae with $E = 1\,\mathrm{GPa}$, $\nu = 0.35$.

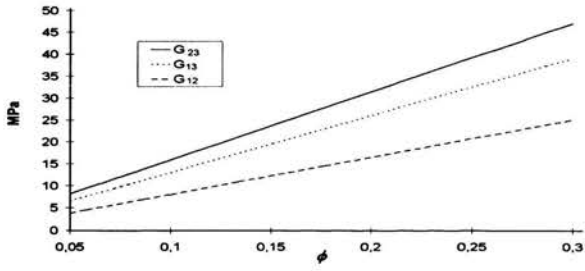

FIGURE 20. Shear moduli in the three orthotropic principal directions versus bone volume fractions; $\alpha = 56/67$, $\beta = 73/134$; isotropic trabeculae with $E = 1\,\mathrm{GPa}$, $\nu = 0.35$.

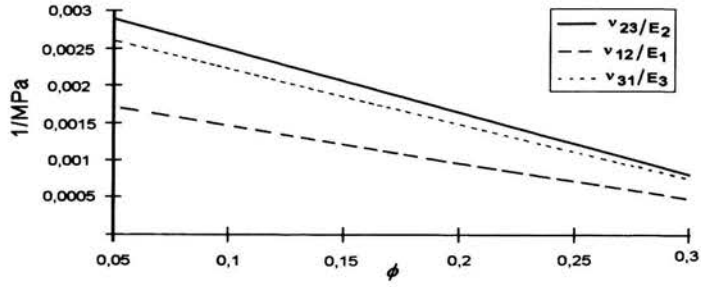

FIGURE 21. Poisson's ratio divided by Young's moduli in the three orthotropic principal directions versus bone volume fraction; $\alpha = 56/67$, $\beta = 73/134$; isotropic trabeculae with $E = 1\,\mathrm{GPa}$, $\nu = 0.35$.

According to Table 9 in [30], the estimates for the elastic modulus of the trabeculae of human cancellous bone vary from 1 to 20 GPa. Future research should be directed towards resolving this problem of great scatter of Young's moduli.

Figures 19-21 correspond to the data listed in the second and third column of Table 4.

7. Rod-like structure

Let now the basic cell Y be given by

$$Y = [-\frac{1}{2}, \frac{1}{2}) \times [-\frac{1}{2}, \frac{1}{2}) \times [-\frac{1}{2}, \frac{1}{2}). \tag{7.1}$$

Due to periodicity the homogenized coefficients do not depend on the basic cell and consequently one may take a translated cell of the basic one. Consequently, we take the translated cell represented in Fig. 22.

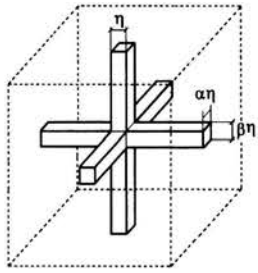

FIGURE 22. Translated rod-like basic cell.

We observe that the thicknesses of three orthogonal struts are not necessarily equal, thus allowing for macroscopically orthotropic response of the trabecular bone. More elaborate and complex rod-like structure, requiring more independent geometrical parameters (or functions) can likewise be envisaged. Let us introduce the following notation:

$$Y_1 = \left\{ \mathbf{y} \in Y, |y_2| \leq \frac{\alpha\eta}{2}, \ |y_3| \leq \frac{\beta\eta}{2} \right\},$$

$$Y_2 = \left\{ \mathbf{y} \in Y, |y_1| \leq \frac{\eta}{2} \text{ and } |y_3| \leq \frac{\beta\eta}{2} \right\},$$

$$Y_3 = \left\{ \mathbf{y} \in Y, |y_1| \leq \frac{\eta}{2} \text{ and } |y_2| \leq \frac{\alpha\eta}{2} \right\},$$

$$Y_{123} = \left\{ \mathbf{y} \in Y, |y_1| \leq \frac{\eta}{2} \text{ and } |y_2| \leq \alpha \frac{\alpha\eta}{2} \text{ and } |y_3| \leq \frac{\beta\eta}{2} \right\},$$

$$Y_\eta^* = Y_1 \cup Y_2 \cup Y_3,$$

$$Y_\eta^* = \eta^2 (\alpha + \beta + \alpha\beta) - 2\eta^3 \alpha\beta.$$

Since $|Y_\eta^*| = (1 + \alpha + \beta)\eta - (\alpha + \beta + \alpha\beta)\eta^2 + \alpha\beta\eta^3$ we get the following estimate

$$\|\mathbf{e}^y(\boldsymbol{\chi}^{(pq)})\|_{L^2(Y_\eta^*)} \leq c\eta. \tag{7.2}$$

Obviously $\boldsymbol{\chi}^{(pq)}$ depend on α, β and η. The constant c is independent of η and

$$e^y(\mathbf{w}) = \frac{1}{2}\left(\frac{w_i}{\partial y_j} + \frac{w_j}{\partial y_i}\right).$$

Using this estimate in (4.3) we conclude that

$$\eta^{-2} C^h_{ijmn} \to C^*_{ijmn}$$

(after extraction of a subsequence if necessary) We can pass to the limit as $\eta \to 0$ in the homogenized equation (4.2), whose solution is denoted by $\mathbf{u}^\eta$. We have

$$u_k^\eta \rightharpoonup u_k^* \quad \text{in } H_0^1(\Omega) \text{ weakly},$$

where $\mathbf{u}^*$ is the solution to the equation:

$$C^*_{ijkn} \frac{\partial^2 u_k^*}{\partial x_j \partial x_n} + (\alpha + \beta + \alpha\beta) f_i = 0 \quad \text{in } \Omega, \qquad \mathbf{u}^* = 0 \quad \text{on } \partial\Omega. \tag{7.3}$$

We observe that now $|Y| = 1$.

Let us pass to finding the limit coefficients C^*_{ijkn}.
Using Eq. (4.3) and the decomposition of Y^* we obtain:

$$\frac{1}{\eta^2} C^h_{ijmn} = \frac{|Y^*|}{\eta^2} C_{ijmn} - \frac{1}{\eta^2} \int_{Y_1} C_{ijpq} \frac{\partial \chi_p^{(mn)}}{\partial y_q} d\mathbf{y} - \frac{1}{\eta^2} \int_{Y_2} C_{ijpq} \frac{\partial \chi_p^{(mn)}}{\partial y_q} d\mathbf{y}$$

$$- \frac{1}{\eta^2} \int_{Y_3} C_{ijpq} \frac{\partial \chi_p^{(mn)}}{\partial y_q} d\mathbf{y} + 2 \frac{1}{\eta^2} \int_{Y_{123}} C_{ijpq} \frac{\partial \chi_p^{(mn)}}{\partial y_q} d\mathbf{y}. \tag{7.4}$$

We have to pass to the limit with $\eta \to 0$ in (7.4), where the integral terms are taken over domains depending on η. To avoid this difficulty we transform Y_1, Y_2, Y_3, and Y_{123} in $\overline{Y}$.
For instance, using the a priori estimate (7.2) and (4.6) we have

$$\int_{Y_1} \left| \mathbf{e}^y \left(\boldsymbol{\chi}^{(pq)} \right) \right| d\mathbf{y} \leq c\eta.$$

Hence, after transformation

$$z_1 = y_1,\ z_2 = (\alpha\eta)^{-1} y_2,\ z_3 = (\beta\eta)^{-1} y_3,$$

and using Korn's inequality, we get

$$\int_Y \left[\left(\frac{\partial \chi_{p1}^{(mn)}}{\partial z_1} \right)^2 + \left((\alpha\eta)^{-1} \frac{\partial \chi_{p1}^{(mn)}}{\partial z_2} \right)^2 + \left((\beta\eta)^{-1} \frac{\partial \chi_{p1}^{(mn)}}{\partial z_3} \right)^2 \right] d\mathbf{z} \leq c_1,$$

where $\chi_{p1}^{(mn)} = \chi_{p1}^{(mn)}(z_1, z_2, z_3) = \chi_p^{(mn)}(z_1, \alpha\eta z_2, \beta\eta z_3)$ and c_1 does not depend on η .
Thus

$$\begin{gathered} \frac{\partial \chi_{p1}^{(mn)}}{\partial z_1} \rightharpoonup h_{p1,1}^{(mn)},\ (\alpha\eta)^{-1} \frac{\partial \chi_{p1}^{(mn)}}{\partial z_2} \rightharpoonup h_{p1,2}^{(mn)}, \\ (\beta\eta)^{-1} \frac{\partial \chi_{p1}^{(mn)}}{\partial z_3} \rightharpoonup h_{p1,3}^{(mn)}, \end{gathered} \tag{7.5}$$

in $L^2(Y)$ weakly. Similarly we have

$$\eta^{-1} \frac{\partial \chi_{p2}^{(mn)}}{\partial z_1} \rightharpoonup h_{p2,1}^{(mn)},\ \frac{\partial \chi_{p2}^{(mn)}}{\partial z_2} \rightharpoonup h_{p2,2}^{(mn)},\ (\beta\eta)^{-1} \frac{\partial \chi_{p2}^{(mn)}}{\partial z_3} \rightharpoonup h_{p2,3}^{(mn)},$$

$$\eta^{-1} \frac{\partial \chi_{p3}^{(mn)}}{\partial z_1} \rightharpoonup h_{p3,1}^{(mn)},\ (\alpha\eta)^{-1} \frac{\partial \chi_{p3}^{(mn)}}{\partial z_2} \rightharpoonup h_{p1,3}^{(mn)},\ \frac{\partial \chi_{p3}^{(mn)}}{\partial z_3} \rightharpoonup h_{p3,3}^{(mn)},$$

$$\eta^{-1} \frac{\partial \chi_{p123}^{(mn)}}{\partial z_1} \rightharpoonup h_{p123,1}^{(mn)},\ (\alpha\eta)^{-1} \frac{\partial \chi_{p123}^{(mn)}}{\partial z_2} \rightharpoonup h_{p123,2}^{(mn)},\ (\beta\eta)^{-1} \frac{\partial \chi_{p123}^{(mn)}}{\partial z_3} \rightharpoonup h_{p123,3}^{(mn)},$$

in $L^2(Y)$ weakly. Here the following notation is used:

$$\chi_{p2}^{(mn)} = \chi_{p2}^{(mn)}(z_1, \eta z_2, z_3) = \chi_p^{(mn)}(\eta z_1, z_2, \beta\eta z_3),$$

$$\chi_{p3}^{(mn)} = \chi_{p3}^{(mn)}(z_1, z_2, z_3) = \chi_p^{(mn)}(\eta z_1, \alpha z_2, z_3),$$

$$\chi_{p123}^{(mn)} = \chi_{p123}^{(mn)}(z_1, z_2, z_3) = \chi_p^{(mn)}(\eta z_1, \alpha\eta z_2, \beta\eta z_3).$$

We observe that due to the periodicity of $\chi_p^{(mn)}$ one has:

$$\int_Y h_{p1,1}^{(mn)}\, d\mathbf{z} = 0,\ \int_Y h_{p2,2}^{(mn)}\, d\mathbf{z} = 0,\ \int_Y h_{p3,3}^{(mn)}\, d\mathbf{z} = 0,$$

Return to (7.4) and let η tend to zero. We get

$$C^*_{ijmn} = (\alpha+\beta+\alpha\beta)\, C_{ijmn} - C_{ijp1} \int\limits_Y (\alpha\beta\, h^{(mn)}_{p2,1} + \beta\, h^{(mn)}_{p3,1})\, d\mathbf{z}$$
$$-C_{ijp2} \int\limits_Y (\alpha\, h^{(mn)}_{p1,2} + \beta\, h^{(mn)}_{p3,2})\, d\mathbf{z} - C_{ijp3} \int\limits_Y (\alpha\beta\, h^{(mn)}_{p2,3} + \alpha\, h^{(mn)}_{p1,3})\, d\mathbf{z} \tag{7.6}$$

To calculate explicitly the integral terms of this formula we take Ψ_j in (4.6) to be a smooth function, Y-periodic and not dependent on y_1. We have the following equations (not independent):

$$C_{2jp2} \int\limits_Y h^{(mn)}_{p1,2}\, dz + C_{2jp3} \int\limits_Y h^{(mn)}_{p1,3}\, dz = -C_{2jmn},$$
$$C_{3jp2} \int\limits_Y h^{(mn)}_{p1,2}\, dz + C_{3jp3} \int\limits_Y h^{(mn)}_{p1,3}\, dz = -C_{3jmn}. \tag{7.7}$$

Similarly taking Ψ_j in (4.6) to be a smooth function, Y-periodic and not dependent on y_2 we obtain

$$C_{1jp1} \int\limits_Y h^{(mn)}_{p2,1}\, dz + C_{1jp3} \int\limits_Y h^{(mn)}_{p2,3}\, dz = -C_{1jmn},$$
$$C_{3jp1} \int\limits_Y h^{(mn)}_{p2,1}\, dz + C_{3jp3} \int\limits_Y h^{(mn)}_{p2,3}\, dz = -C_{3jmn}. \tag{7.8}$$

Suppose now that Ψ_j in (4.6) is a smooth function, Y-periodic and not dependent on y_3. Then we get

$$C_{1jp1} \int\limits_Y h^{(mn)}_{p3,1}\, dz + C_{1jp2} \int\limits_Y h^{(mn)}_{p3,2}\, dz = -C_{1jmn},$$
$$C_{2jp1} \int\limits_Y h^{(mn)}_{p3,1}\, dz + C_{2jp2} \int\limits_Y h^{(mn)}_{p3,2}\, dz = -C_{2jmn}. \tag{7.9}$$

The above equations enable us to obtain the components of the matrix $\mathbf{C}^*$. In the case of isotropic material with the Lamé constants λ, μ and assuming that $\alpha = \beta = 1$ we finally get:

$$\mathbf{C}^* = \begin{bmatrix} \frac{10\mu^2+15\mu\lambda+6\lambda^2}{\mu+\lambda} & 6\lambda & 6\lambda & 0 & 0 & 0 \\ 6\lambda & \frac{10\mu^2+15\mu\lambda+6\lambda^2}{\mu+\lambda} & 6\lambda & 0 & 0 & 0 \\ 6\lambda & 6\lambda & \frac{10\mu^2+15\mu\lambda+6\lambda^2}{\mu+\lambda} & 0 & 0 & 0 \\ 0 & 0 & 0 & 12\mu & 0 & 0 \\ 0 & 0 & 0 & 0 & 12\mu & 0 \\ 0 & 0 & 0 & 0 & 0 & 12\mu \end{bmatrix}$$

and

$$\mathbf{C}^h = \frac{1}{3}\, \phi\, \mathbf{C}^*,$$

where ϕ is the volume fraction of material. The general formula for the effective rod-like (strut-like) cellular solid can be used to the estimation of elastic moduli of trabecular bone with such an architecture.

Similar problem of determination of macroscopic moduli of cancellous bone with rod-like architecture was also considered in [83, 86],where an approximate procedure was used.

8. Honeycomb structure

Let us pass to estimation of the macroscopic effective elastic moduli C^h_{ijkl} for cancellous bone with honeycomb architecture, cf. Fig. 23.

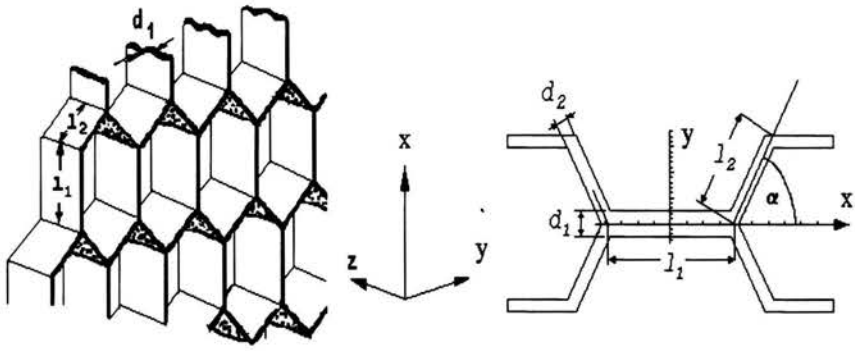

FIGURE 23. Honeycomb architecture.

These moduli are determined in an approximate manner for small volume fraction ϕ characterizing the solid phase. For the sake of simplicity we assume that $d_1 = d_2$. To determine the effective moduli C^h_{ijkl}, we exploit approximate solutions of the local problem (4.4). The effective technical coefficients, given by Eqs. (6.2)-(6.4), are calculated by using formulae for C^h_{ijkl} specified by (4.3). After lenghtly calculations we obtain

$$C^h_{1111} = \frac{(a_3)^2 \cos^2\alpha}{m_1} E\,\phi + 8\,\frac{(a_3)^4\,(c_2)^2}{m_2} E\phi^3\,, \tag{8.1}$$

$$C^h_{2222} = \frac{\sin^4\alpha}{m_1} E\phi - 8\,\frac{(a_3)^4 \sin^4\alpha\,(c_1)^2}{m_2} E\phi^3\,, \tag{8.2}$$

$$C^h_{1122} = \frac{a_3 \cos\alpha\, \sin^2\alpha}{m_1} E\phi + 8\,\frac{(a_3)^4\, \sin^2\alpha\, c_1\, c_2}{m_2} E\phi^3\,, \tag{8.3}$$

$$C^h_{1133} = \frac{a_1\, a_3 \cos\alpha}{m_1} \nu\, E\phi + 8\,\frac{(a_3)^4\, b_1\, c_2\,(2+\xi)}{m_2} \nu\, E\phi^3\,, \tag{8.4}$$

$$C^h_{2233} = \frac{a_1 \sin^2\alpha}{m_1}\,\nu\,E\phi + 8\,\frac{(a_3)^4\,b_1\,c_2\,\sin^2\alpha\,(2+\xi)}{m_2}\,\nu\,E\phi^3\,, \tag{8.5}$$

$$C^h_{3333} = \left(1 + \frac{\nu^2 {a_1}^2}{m_1}\right) E\phi + 8\,\frac{(a_3)^4\,(b_1)^2\,(2+\xi)^2}{m_2}\,\nu^2\,E\phi^3\,, \tag{8.6}$$

$$C^h_{1212} = 4\,\frac{(a_3)^2\left(a_3 - (\cos(\alpha))^2\,\xi\right)(\sin(\alpha))^2\left(a_3 + (\sin(\alpha))^2\,\xi\right)}{\xi^2\,(2+\xi)^3\,(2\xi+1)}\,E\,\phi^3\,, \tag{8.7}$$

$$C^h_{1313} = 2\,\frac{a_1\,a_3}{\xi\,(2+\xi)^2}\,\mu\,\phi\,, \tag{8.8}$$

$$C^h_{2323} = 2\,\frac{a_3\,\sin^2\alpha}{(2+\xi)\,a_1}\,\mu\,\phi\,. \tag{8.9}$$

The remaining moduli disappear. In the above formulae the following notation is used:

$$a_1 = 1 + \xi\,\cos(\alpha)\,, \quad a_2 = 1 + 2\,(\cos(\alpha))^2\,\xi\,, \quad a_3 = \xi + \cos(\alpha)\,,$$

$$b_1 = -1 + 2\,\cos(\alpha)\,, \quad b_2 = -1 + 2\,(\cos(\alpha))^3\,,$$

$$c_1 = 2\,(2+\xi)\,\cos\alpha - \nu^2\,a_1\,, \quad c_2 = b_2\,(2+\xi) + \nu^2\,a_1\,\sin^2\alpha\,,$$

$$m_1 = (2+\xi)\,a_2 - \nu^2\,(a_1)^2\,, \quad m_2 = (2+\xi)^3\,(m_1)^2\,,$$

$$\xi = \frac{l_1}{l_2}.$$

The effective technical moduli are given by:

$$E^h_x = 8\,\frac{(\xi+\cos\alpha)^4}{(2+\xi)^3}\,E\,\phi^3\,, \quad E^h_y = 8\,\frac{(\xi+\cos\alpha)^2\,\sin^4\alpha}{\cos^2\alpha(2+\xi)^3}\,E\,\phi^3\,, \quad E^h_z = E\,\phi\,,$$

$$\nu^h_{xy} := \frac{(\sin(\alpha))^2}{\cos(\alpha)\,a_3} + 8\,\frac{\sin^2\alpha\,b_2\,a_3}{\cos^3\alpha\,(2+\xi)^2}\,\phi^2\,,$$

$$\nu^h_{yx} = \frac{a_3\,\cos\alpha}{(\sin(\alpha))^2} - 16\,\frac{\cos(\alpha)(a_3)^4}{(\sin(\alpha))^2\,(2+\xi)^2}\,\phi^2,$$

$$\nu^h_{xz} = \nu^h_{yz} = \nu\,,$$

$$\nu^h_{zx} := 8\,\frac{(a_3)^4\nu}{(2+\xi)^3}\,\phi^2\,,$$

$$\nu^h_{zy} = 8\,\frac{\nu\,(\sin(\alpha))^4\,(a_3)^2}{(2+\xi)^3\,(\cos(\alpha))^2}\,\phi^2,$$

$$\frac{G^h_{xz}}{\mu} = C^h_{1313}\,, \quad \frac{G^h_{yz}}{\mu} = C^h_{2323}\,, \quad \frac{G^h_{xy}}{E} = C^h_{1212}\,.$$

Table 5 gathers some available data concerning the values of elastic modulus of individual trabeculae, cf. [30, 31]. These data were used to depict the dependence of the elastic moduli on various parameters, cf. Figs. 24-29.

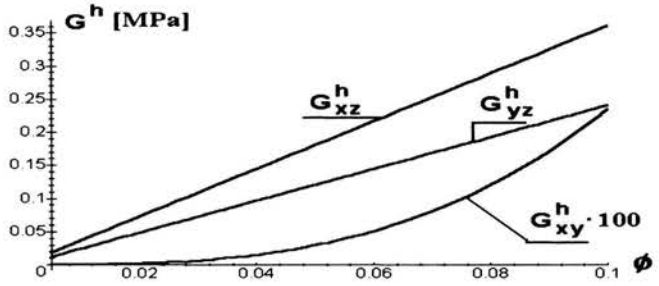

FIGURE 24. Effective shear moduli versus volume fraction; $E = 20\,\mathrm{GPa}$, $\xi = 2$, $\alpha = \pi/3$, $\nu = 0.3$.

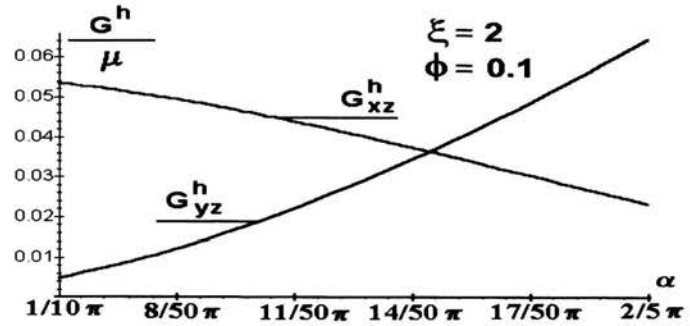

FIGURE 25. Effective shear moduli versus α.

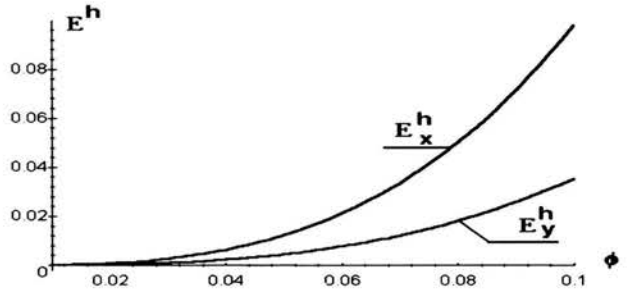

FIGURE 26. Effective Young moduli versus volume fraction; $E = 20\,\mathrm{GPa}$, $\xi = 2$, $\alpha = \pi/3$, $\nu = 0.3$.

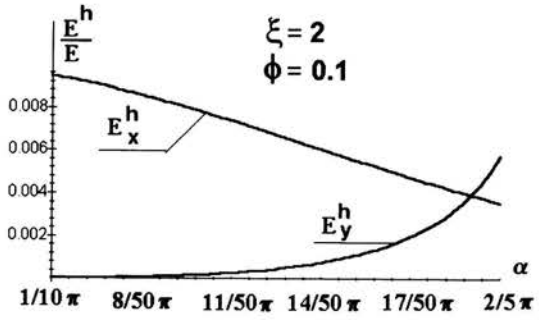

FIGURE 27. Effective Young moduli versus α.

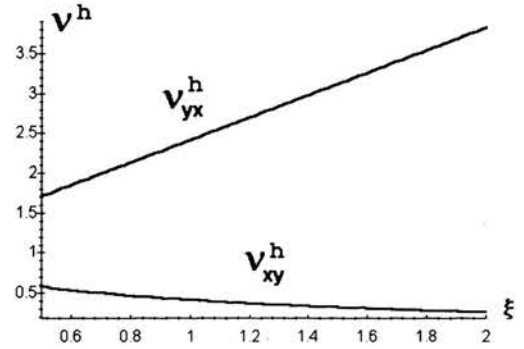

FIGURE 28. Effective Poisson ratio versus fraction $\xi = l_1/l_2$; $E = 20\,\mathrm{GPa}$, $\alpha = \pi/4$, $\nu = 0.3$.

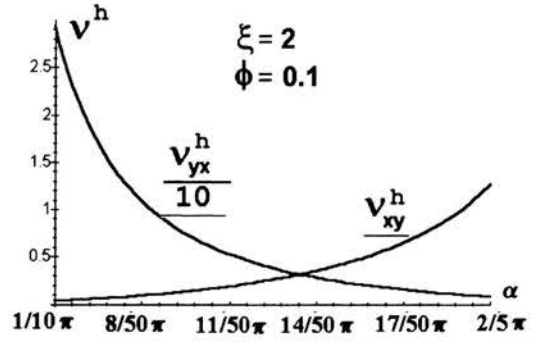

FIGURE 29. Effective Poisson ratio versus versus α; $E = 20\,\mathrm{GPa}$, $\nu = 0.3$.

TABLE 5. Elastic modulus of individual trabecular, after [30, 31].

Source	*Type of bone*	*Analytical/ test method*	*Estimate of trabeculae elastic modulus*
Wolff	Human Bovine		17 to 20 GPa (wet) 18 to 22 GPa (wet)
Pugh *et al.*	Human, distal femur	Finite elenent method	Concluded that the modulus of the trabeculae was less than the modulus of compact bone
Townsend *et al.*	Human, proximal tibia	Inelastic buckling	11.38 GPa (wet) 14.13 GPa (dry)
Ashman and Rho	Bovine femur Human femur	Ultrasonic test method Ultrasonic test method	10.90 1.6 GPa (wet) 12.7 2.0 GPa (wet)
Runkle and Pugh	Human, distal femur	Buckling	8.69 3.17 GPa (dry)
Mente and Lewis	Dried human femur Fresh frozen human tibia	Experimental with finite element method	5.3 2.6 GPa
Kuhn *et al.*	Fresh frozen human tibia	Three-point bending of ultra small machined specimens	3.17 1.5 GPa
Williams and Lewis	Human, proximal tibia	Experiment with 2-D finite element method	1.30 GPa
Rice *et al.*	Bovine	Statist. data analysis model of Christensen	0.61 GPa
Ryan and Williams	Fresh bovine femur	Tension test, single trabeculae	0.76 0.39 GPa
Rice *et al.*	Human	Statist. data analysis, model of Christensen	0.61 GPa

9. Torsional creep and relaxation of cancellous bone filled with marrow

As we already know trabecular bone is a porous structure consisting of bony network of connecting rods, plates and prisms (elastic phase) filled with bone marrow (viscous phase) [38]. We are also aware that various approaches to modeling the mechanical behavior of trabecular bone have been proposed, see for instance [38], [45] and [96] and the previous sections of our paper. In this section the structural model developed earlier by us in [77] is applied to predict the creep and relaxation behavior of long bone under torsion.

To this end we introduce : λ_0, μ_0 – the elastic moduli of compact bone; λ_1, μ_1 – the elastic moduli of a trabecular bone; λ_2, μ_2 – the bulk and shear viscosities of bone marrow, λ_2^*, $\mu_2^* = I\omega\mu_2$ – the complex moduli of marrow;

μ^*_{eff} – the homogenized (effective) complex modulus of cancellous bone, μ^*_{app} – the apparent complex modulus of bone, $\Phi_{\text{eff}}(t)$ and $\Psi_{\text{eff}}(t)$ – the effective creep and relaxation functions of the cancellous bone, $\Phi^*_{\text{app}}(t)$ and $\Psi^*_{\text{app}}(t)$ – the apparent creep and relaxation functions of long bone, φ – the relative apparent density of cancellous bone.

9.1. Basic equations

Let us consider an idealized model of cancellous bone represented by an elastic rod reinforced with cylindrical viscoelastic fibers arranged in a hexagonal lattice. Different arrangement of fibres can also be considered. According to the notation introduced above, λ_1 and μ_1 are the Lamé constants of the matrix, while λ_2^* and μ_2^* denote the Lamé coefficients of fibers. By using the homogenization procedure, the equations defining the effective torsion modulus μ_{eff}/μ_1 are given by, cf. [87],

$$\frac{\mu^*_{\text{eff}}}{\mu_1} = \frac{1}{|Y|}\int\limits_Y \mu(y)\frac{\partial T(y)}{\partial y_1}dy, \quad \mu(y) = \begin{cases} \mu_1 \text{ if } y \in \Omega_1, \\ \mu_2^* \text{ if } y \in \Omega_2, \end{cases},$$

$$\frac{\partial}{\partial y_1}\left(\mu(y)\frac{\partial T(y)}{\partial y_1}\right) + \frac{\partial}{\partial y_2}\left(\mu(y)\frac{\partial T(y)}{\partial y_2}\right) = 0, \tag{9.1}$$

$$\frac{1}{|Y|}\int\limits_Y \frac{\partial T(y)}{\partial y_1}dy = 1, \ \frac{1}{|Y|}\int\limits_Y \frac{\partial T(y)}{\partial y_2}dy = 0, \quad \frac{\partial T(y)}{\partial y} - Y - \text{periodic},$$

where $\Omega_1$and Ω_2 are the domains occupied by the elastic matrix and viscoelastic fibres, respectively. The macroscopic modulus $(\mu^*_{\text{eff}}/\mu_1) - 1$ has an asymptotic expansion at $y = 0$

$$\mu^*_{\text{eff}}/\mu_1 - 1 = \varphi y - \frac{1}{2}\varphi(1-\varphi)y^2 + O(y^3), \tag{9.2}$$

and attains discrete values indicated in Table 6, cf. [64].

TABLE 6. Discrete values of the elastic torsional modulus $\mu_{\text{eff}}/\mu_1 - 1$ for hexagonal array of cylinders, after [64].

x_i	$\varphi = 0.76$	$\varphi = 0.80$	$\varphi = 0.84$	$\varphi = 0.88$
$x_{-1} = -1$	-0.8711	-0.8996	-0.9286	-0.9607
$x_0 = 0$	0.0000	0.0000	0.0000	0.0000
$x_1 = 9$	3.3778	3.9489	4.6887	5.7225
$x_2 = 49$	5.7076	7.2600	9.7931	15.1565
$x_3 = \infty$	6.7600	8.9586	13.0093	24.4508

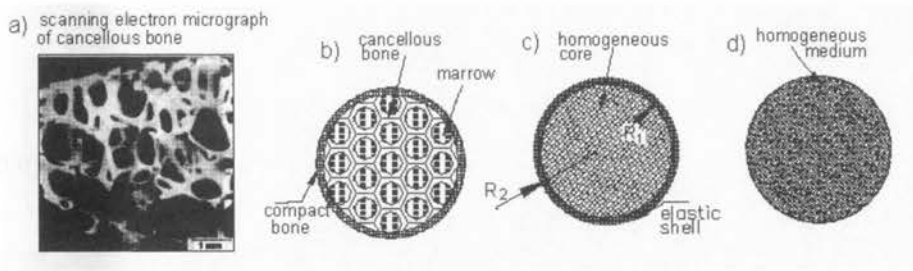

FIGURE 30. Main steps of modeling of the torsional properties of typical human bone: a) micrograph showing cellular structure of cancellous bone, after [39], b) idealized microstructural model of cancellous bone, c) two-phase continuous model obtained via homogenization of cancellous core, d) homogeneous medium modeling long human bone.

In addition, $(\mu^*_{\text{eff}}/\mu_1) - 1$ has Stieltjes integral representation introduced in [87] in the form

$$\frac{\mu^*_{\text{eff}}}{\mu_1} - 1 = z f_1(z) = \int_0^{1/(1+x_i)} z \frac{d\beta(x_i,\xi)}{1+(z-x_i)\xi}, \quad z = \frac{\mu^*_2}{\mu_1} - 1. \tag{9.3}$$

This representation generalizes that derived by Bergman [23] and rederived in a more general form by Golden and Papanicolaou in [41]. For more details on application of Stieltjes function to the estimation of effective moduli the reader is referred to [80]-[83], [85] and [86].

9.2. Continued fraction bounds on torsional modulus

Let us let us consider now bounds on the effective complex modulus $(\mu^*_{\text{eff}}(z)/\mu_1) - 1$, $z = i\frac{\omega\mu_2}{\mu_1} - 1$.

Let us introduce the sequence of complex bounds $F_j(z,\tau)$ on $\mu^*_{\text{eff}}(z)/\mu_1 - 1$ given by

$$zF_j(z,\tau) = \cfrac{zg_0}{1+zg_1+\cfrac{zg_2}{1+\cfrac{zg_3}{1+\cfrac{(z-x_1)g_4}{1+(z-x_2)V_jF(z,\tau)}}}}, \quad j = 0,1,2,\ldots \tag{9.4}$$

where the elementary bound $F(z,\tau)$ appearing in (9.4) takes the form, cf. [19],

$$F(z,\tau) = \begin{cases} \dfrac{(1-\tau)}{1+z\tau}, & \text{if} \quad 0 \le \tau \le 1, \\ (1+\tau), & \text{if} \quad -1 \le \tau \le 0. \end{cases} \tag{9.5}$$

From (9.4) we obtain

$$
\begin{aligned}
zF_0(z,\tau) &= F(z,\tau),\\
zF_1(z,\tau) &= \frac{zg_0}{1+zV_1F(z,\tau)},\\
zF_2(z,\tau) &= \frac{zg_0}{1+zg_1+zV_2F(z,\tau)},
\end{aligned}
\tag{9.6}
$$

where the renormalizing coefficients V_j satisfy the equations, cf. Table 6,

$$
-F_1(-1,0) = (\mu^*_{\text{eff}}(-1)/\mu_1) - 1. \tag{9.7}
$$

In order to evaluate the coefficients g_j, $j = 0,1,2,\ldots,5$, generating via (9.4) the bounds on $\mu^*_{\text{eff}}(z)/\mu_1 - 1$ the following input data are available: from (9.2) and Table 6, for $\varphi = 0.88$, we have,

$$
\begin{aligned}
&\frac{d}{dz}F_5(z,0)|_{z=x_0} = \varphi = 0.88,\\
&\frac{d^2}{dz^2}F_5(z,0)|_{z=x_0} = 0.5\varphi(1-\varphi) = -0.0528,\\
&F_5(x_{-1},0) = -0.961, \qquad F_5(x_1,0) = 5.722,\\
&F_5(x_2,0) = 15.156, \qquad F_5(x_3,0) = 24.45.
\end{aligned}
\tag{9.8}
$$

Similar input data were obtained for $\varphi = 0.76$, $\varphi = 0.80$, and $\varphi = 0.84$. The evaluated coefficients g_j are listed in Table 7.

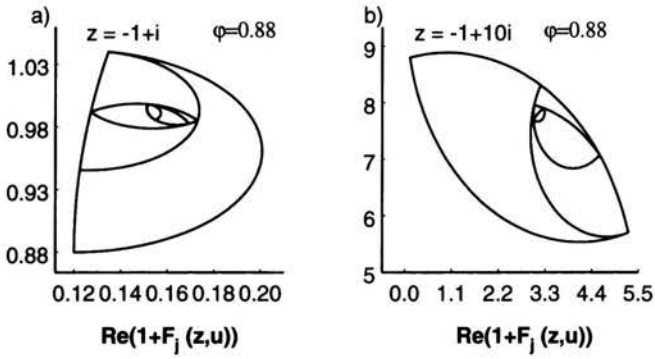

FIGURE 31. The sequence of lens-shaped bounds $1+zF(z,\tau)$, $1+zF_1(z,\tau),\ldots,$ $1+zF_5(z,\tau)$ on the torsional complex modulus μ^*_{eff}/μ_1 for the idealized structural model of cancellous bone.

TABLE 7. The continued fraction coefficients $g_j, j = 1, 2, \ldots, 5$ and V_5.

φ	g_0	g_1	g_2	g_3	g_4	V_5
0.76000	0.76000	0.11242	0.00757	0.46475	0.00024	0.01928
0.80000	0.80000	0.08929	0.01070	0.43494	0.00029	0.01954
0.84000	0.84000	0.06456	0.01543	0.38244	0.00052	0.01955
0.88000	0.88000	0.02400	0.03599	0.28841	0.00127	0.01939

The bounds $1+zF(z,\tau)$, $1+zF_1(z,\tau)$, $\ldots$, $1+zF_5(z,\tau)$, $z = -1+i$, $\varphi = 0.88$, have also been evaluated and depicted in Fig. 31. Figure 32 presents, for 0.88 the multipoint Padé approximants $1 + zF_5(z,0)$ and $1 + zF_5(z,1)$, $z = -1+i\omega$, $\omega = 1, 10, \ldots, 2000$, estimating the torsional modulus $\mu^*_{\text{eff}}(z)/\mu_1$.

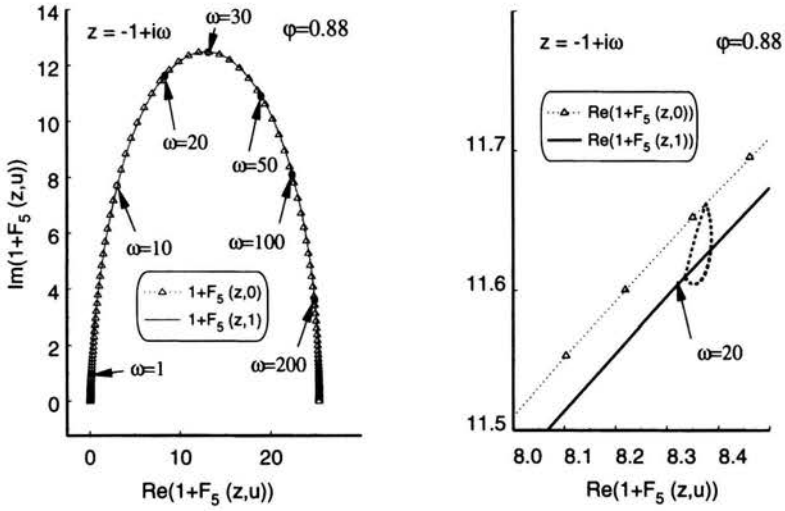

FIGURE 32. Complex torsional modulus of the elastic beam filled with viscous fluid and evaluation error (idealized model of cancellous bone, $\varphi = 0.76$, 0.80, 0.84, 0.88). Normalizing coefficients are: $\mu_2 = 0.0067\,\text{kg}\,\text{m}^{-1}\text{s}^{-1}$ and $\mu_1 = 3.3\,\text{GN}\,\text{m}^{-2}$, after [6].

9.3. Multipoint Padè approximants

According to the definitions given in [19] and [20] the rational functions $1 + [3/3] = 1 + F_j(z,0)$ and $1 + [2/2] = 1 + zF_j(z,1)$ considered above are the multipoint Padé approximants to the effective complex modulus μ^*_{eff}/μ_1. Those approximants have been evaluated explicitly in [87] and depicted in Table 8.

Now we are in a position to introduce an inclusion regions Γ_j, i.e. the region in the complex plane surrounded by the bounds $1 + F_j(z,\tau)$. It can

TABLE 8. Multipoint Padé approximants $1 + zF_5(z,0)$ to torsional modulus μ_{eff}/μ_1 of hexagonal array of viscous cylinders embedded in elastic matrix; φ-the volume fraction

φ	$1 + zF_5(z,0)$	$1 + zF_5(z,1)$
0.76	$\frac{1 + 1.7328z + 0.9159z^2 + 0.1476z^3}{1 + 0.9728z + 0.2678z^2 + 0.0190z^3}$	$\frac{1 + 1.3460z + 0.4066z^2}{1 + 0.5860z + 0.0524z^2}$
0.80	$\frac{1 + 1.8655z + 1.0787z^2 + 0.1910z^3}{1 + 1.0655z + 0.3063z^2 + 0.0192z^3}$	$\frac{1 + 1.3364z + 0.3881z^2}{1 + 0.5364z + 0.0390z^2}$
0.84	$\frac{1 + 1.8901z + 1.0865z^2 + 0.1816z^3}{1 + 1.0501z + 0.2717z^2 + 0.0130z^3}$	$\frac{1 + 1.3048z + 0.3481z^2}{1 + 0.4648z + 0.0249z^2}$
0.88	$\frac{1 + 1.8582z + 1.0009z^2 + 0.1345z^3}{1 + 0.9782z + 0.1929z^2 + 0.0053z^3}$	$\frac{1 + 1.2331z + 0.2685z^2}{1 + 0.3531z + 0.0106z^2}$

easily be proved that for the problem considered we have

$$\begin{aligned} &\mu^*_{\text{eff}}/\mu_1 \in \Gamma_5 \in \Gamma_4 \in \Gamma_3 \in \Gamma_2 \in \Gamma_1, \\ &1 + zF_5(z,0) \in \Gamma_5 \in \Gamma_4 \in \Gamma_3 \in \Gamma_2 \in \Gamma_1, \\ &1 + zF_5(z,1) \in \Gamma_5 \in \Gamma_4 \in \Gamma_3 \in \Gamma_2 \in \Gamma_1. \end{aligned} \tag{9.9}$$

Since Γ_5 is very narrow (the smallest regions in Fig. 31a,b), we can assume that the Padé approximant $1 + zF_5(z,0)$ provides a good estimate of the effective torsional modulus μ^*_{eff}/μ_1. Hence we conclude that the function

$$\mu^*_{\text{eff}}/\mu_1 = 1 + zF_5(z,0), \quad \varphi \leq 0.88 \tag{9.10}$$

solves the boundary value problem (9.3) with satisfactory accuracy. The torsional modulus given by (9.10) is presented in Table 9 and depicted in Fig.33.

Now we are in a position to investigate the influence of marrow on the real part of the complex torsion modulus. To this end we use the characteristic time $\tau = \mu_2/\mu_1 = \frac{0.67}{3.3\cdot 10^9}\frac{\text{Poise}\times\text{m}^2}{\text{N}} = 2.03 \cdot 10^{-11}$s. From Fig. 33 follows that the hydraulic stiffening starts for $\omega\tau \approx 5$. Hence we immediately obtain: $\omega = 5/(2.03\cdot 10^{-11}\text{ s}) = 2.463\cdot 10^{11}$ Hz. The effect of the presence of the bone marrow is observable for very high oscillating frequency exceeding $2.463 \cdot 10^{11}$ Hz. On account of that the influence of bone marrow can be neglected in physiological situations.

The value obtained should be treated with caution since the considered model of torsion of long bone is constituted of both the compact and cancellous bone. More refined models are required to better estimate the influence of marrow on the mechanical behavior of long bone.

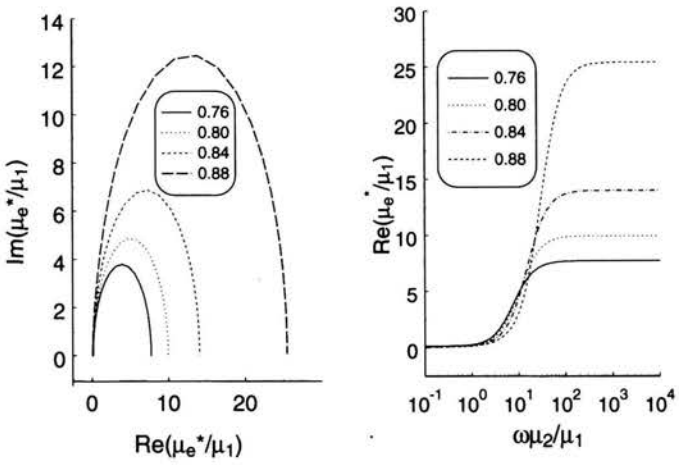

FIGURE 33. Complex torsional modulus and its real part for the model of cancellous bone (the elastic beam filled with viscous fibers); $\varphi = 0.76, 0.80, 0.84, 0.88$. Normalizing coefficients are: $\mu_2 = 0.0067\,\mathrm{kg\,m^{-1}s^{-1}}$ and $\mu_1 = 3.3\,\mathrm{GN\,m^{-2}}$, after [39].

TABLE 9. The torsional modulus μ_*/μ_1 for the inhomogeneous beam filled with the viscous fibres distributed in hexagonal array of cylinders

φ	$\mu^*_{\mathrm{eff}}/\mu_1 = 1 + zF_5(z,0), \quad z = \frac{I\omega}{\varkappa} - 1, \quad \varkappa = \frac{\mu_1}{\mu_2}$
0.76	$7.760 - \dfrac{60.980\varkappa}{10.09\varkappa - I\omega} - \dfrac{0.0974\varkappa}{4.157\varkappa - I\omega} - \dfrac{0.0431\varkappa}{2.831\varkappa - I\omega}$
0.80	$9.957 - \dfrac{102.62\varkappa}{12.56\varkappa - I\omega} - \dfrac{0.1831\varkappa}{3.814\varkappa - I\omega} - \dfrac{.0218\varkappa}{2.603\varkappa - I\omega}$
0.84	$14.01 - \dfrac{209.39\varkappa}{17.27\varkappa - I\omega} - \dfrac{0.4192\varkappa}{4.210\varkappa - I\omega} - \dfrac{0.0192\varkappa}{2.477\varkappa - I\omega}$
0.88	$25.45 - \dfrac{737.96\varkappa}{31.67\varkappa - I\omega} - \dfrac{1.6569\varkappa}{5.446\varkappa - I\omega} - \dfrac{.02234\varkappa}{2.388\varkappa - I\omega}$

9.4. Torsional creep and relaxation functions

The modulus $\mu(z)/\mu_1$ and compliance $\mu_1/\mu^*(z)$, $z = (I\omega/\varkappa) - 1$, $\varkappa = \mu_1/\mu_2$, divided by $I\omega$ are the Fourier transforms of the torsional creep function $\Phi(t)$ and torsional relaxation function $\Psi(t)$, respectively, cf. [26].

TABLE 10. The torsional modulus μ_1/μ_* for the inhomogeneous beam filled with the viscous fibers distributed in hexagonal array of cylinders.

φ	$\mu_1/\mu^*_{\text{eff}} = 1 + zF_5(z,0), \quad z = \frac{I\omega}{\varkappa} - 1, \quad \varkappa = \frac{\mu_1}{\mu_2}$
0.76	$0.129 + \frac{0.0146\varkappa}{4.196\varkappa - I\omega} + \frac{0.0655\varkappa}{2.887\varkappa - I\omega} + \frac{0.9348\varkappa}{2.124\varkappa - I\omega}$
0.80	$0.100 + \frac{0.0476\varkappa}{3.911\varkappa - I\omega} + \frac{0.0666\varkappa}{2.643\varkappa - I\omega} + \frac{0.9226\varkappa}{2.095\varkappa - I\omega}$
0.84	$0.071 + \frac{0.07551\varkappa}{4.397\varkappa - I\omega} + \frac{0.0925\varkappa}{2.521\varkappa - I\omega} + \frac{0.9011\varkappa}{2.066\varkappa - I\omega}$
0.88	$0.039 + \frac{0.1339\varkappa}{5.956\varkappa - I\omega} + \frac{0.1471\varkappa}{2.450\varkappa - I\omega} + \frac{0.8608\varkappa}{2.034\varkappa - I\omega}$

Hence we can write

$$\mu_1\overline{\Phi(I\omega)} = \frac{\mu_1}{I\omega\mu^*(z)(z)}, \quad \frac{\overline{\Psi(I\omega)}}{\mu_1} = \frac{\mu^*(z)(z)}{I\omega\mu_1}, \quad z = \frac{I\omega\mu_2}{\mu_1} - 1. \tag{9.11}$$

The inverse of the Fourier transformations of $\overline{\Phi(I\omega)}$ and $\overline{\Psi(I\omega)}$ take the forms, cf. Table 11 and Eq. (9.11)

$$\begin{aligned} \mu_1\Phi(t) &= d^c + \sum_{n=1}^{3} \frac{b_n^c}{a_n^c}\left(1 - e^{-\varkappa a_n^c t}\right), \\ \frac{\Psi(t)}{\mu_1} &= d^r - \sum_{n=1}^{3} \frac{b_n^r}{a_n^r}\left(1 - e^{-\varkappa a_n^r t}\right). \end{aligned} \tag{9.12}$$

Here the coefficients $d^c, d^r, b_n^c, b_n^r, a_n^c$ and a_n^r take the values provided in Table 11.

TABLE 11. Coefficients for the evaluation of torsional creep and relaxation functions, the input data for (9.12).

φ	d^c	b_1^c	b_2^c	b_3^c	a_1^c	a_2^c	a_3^c
0.76	0.1289	0.0146	0.0655	0.9348	2.1958	0.8867	0.1238
0.80	0.1004	0.0476	0.0666	0.9226	1.9109	0.6432	0.0948
0.84	0.0714	0.0755	0.0925	0.9011	2.3972	0.5213	0.0656
0.88	0.0393	0.1339	0.1471	0.8608	3.9565	0.4500	0.0344
φ	d^r	b_1^r	b_2^r	b_3^r	a_1^r	a_2^r	a_3^r
0.76	7.7600	60.980	0.0974	0.0431	8.0939	2.1575	0.8312
0.80	9.9586	102.62	0.1831	0.0218	10.557	1.814	0.6035
0.84	14.009	209.39	0.4192	0.0192	15.275	2.2101	0.4768
0.88	25.451	737.96	1.6569	0.0223	29.669	3.4456	3.4456

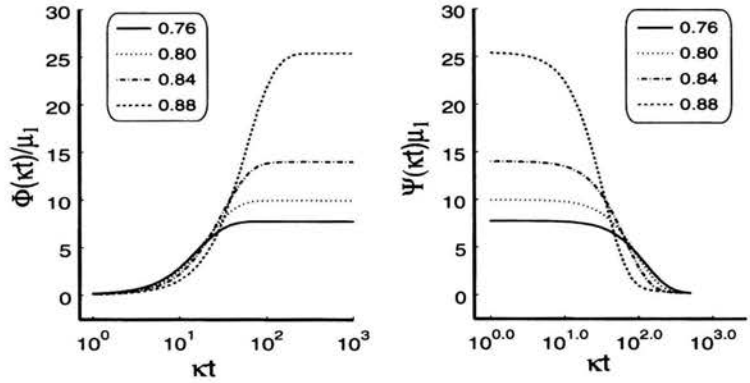

FIGURE 34. The torsional creep function $\Phi(t)$ and relaxation function $\Psi(t)$ for the porous beam consisting of hexagonal array of viscous fibers spaced in the elastic matrix. Normalizing coefficients are: $\mu_2 = 0.0067\,\mathrm{kg\,m^{-1}s^{-1}}$ and $\mu_1 = 3.3\,\mathrm{GN\,m^{-2}}$, after [38].

For cancellous bone we have $\varkappa = 1/\tau = 4.926 \times 10^{10} s^{-1}$. From Fig. 34 follows that the hydraulic stiffening starts for $\varkappa t_s \approx 5$. Hence $t_s = 5/4.926 \times 10^{10} = 1.015 \times 10^{-10} s$. On account of that the influence of bone marrow on creeping and relaxation of cancellous bone is negligible.

10. Concluding remarks

The aim of this comprehensive paper was to synthesize our results pertaining to macroscopic modeling of compact and cancellous bone by using homogenization methods.

In compact bone three distinct levels were distinguished. To find the elastic macroscopic moduli, reiterated homogenization was applied.

Cancellous bone was modeled as a cellular solid. Three types of cellular structures were considered: plate-like, rod-like, and honeycomb. Obviously, periodic microstructures are an idealization of real bone tissue. Each of the models proposed involves several geometrical parameter thus ensuring certain flexibility in applications. Trabeculae were assumed to be isotropic, according to available axperimental data. General formula (4.3) for the determination of the homogenized elastic moduli of porous elastic materials enables to cope with very complex microstructures of cancellous bone. For instance, the geometry of trabeculae can be described by several independent parameters or functions. Then, however, the difficult problem is to solve the periodic cell problem (4.4), (4.5) or (4.6). For more complex (periodic) architectures such a problem can only be solved numerically, cf. [51].

As is well-known, bone is an inhomogeneous material. Inhomogeneity can easily be included in homogenization procedures for bone, since then, for instance, the elastic moduli C_{ijkl} appearing in (2.1) depend on the local variables and macroscopic variable $\mathbf{x}$. In this case the homogenized moduli C^h_{ijkl} also depend on $\mathbf{x} \in \Omega$, cf. also (2.1), (2.11).

A broader class of microstructures requires using stochastic homogenization, cf. [73, 74]. We observe that periodic homogenization is a specific case of the stochastic homogenization. To characterize cancellous bone treated as a porous material with random distribution of microinhomogenities (pores) one can use the geometry of random fields. For an excellent review the reader is referred to the comprehensive paper by Adler and Thovert [1], cf. also [74].

The third topic presented in this paper concerns influence of marrow on long human bone behaviour under torsion. By using Padé approximants and continued fraction technique the analytical formulae predicting the hydraulic stiffening of a human bone due to the presence of marrow were obtained. According to the presented model, the mechanical role of marrow in physiological loads of frequences is negligible.

Acknowledgement

This work was supported by EC through the project MIAB, contract QLK6-CT-1999-02024.

References

1. P.M. ADLER and J.-F. THOVERT, *Real porous media: local geometry and macroscopic properties*, Appl. Mech. Reviews, pp.537-585, 1998.
2. G. ALLAIRE and H. BRIANE, *Multiscale convergence and reiterated homogenization*, Proc. R. Soc. Edinburgh, Vol.126A, pp.297-342, 1996.
3. B. AOUBIZA, *Homogenéisation d'un composite multi-échelle: application à une modélisation numérique de l'os haversien compact*, Thèse, Université de Franche-Comté, 1991.
4. B. AOUBIZA, J.M.CROLET and A. MEUNIER, *On the mechanical characterization of compact bone structure using the homogenization theory*, J. Biomech., Vol.29 , 1539-1547, 1996.
5. A. ASCENZI, M.G. ASCENZI, A. BENVENUTI and F. MANGO, *Pinching in longitudinal and alternate osteons during cyclic loading*, J. Biomech., Vol.30, pp.689-695, 1997.
6. A. ASCENZI, P. BASCHIERI and A. BENVENUTI, *The bending properties of single osteons*, J. Biomech., Vol.23, pp.763-771 1990.
7. A. ASCENZI, P. BASCHIERI and A. BENVENUTI, *The torsional properties of single selected osteons*, J. Biomech., Vol.27, pp.875-884, 1994.

8. A. ASCENZI, A. BENVENUTI, F. MANGO and R. SIMILI, *Mechanical hysteresis loops from single osteons: technical devices and preliminary results*, J. Biomech., Vol.18, pp.391-398, 1985.

9. A. ASCENZI, A. BIGI, M.H.J. KOCH, A. RIPAMONTI and N. ROVENI, *A low- angle X-ray diffraction analysisof osteonic inorganic phase using synchrotron radiation*, Calc. Tissue Int., Vol.37, pp.659-664, 1985.

10. A. ASCENZI, A. BIGI, A. RIPAMONTI and N. RIVERI, *X-ray diffraction analysis of transversal osteonic lamellae*, Calcif, Tissue Int., Vol.35, pp.279-283, 1983.

11. A. ASCENZI and E. BONUCCI, *The tensil properties of single osteons*, Anat. Record, Vol.158, pp.375-386, 1967.

12. A. ASCENZI and E. BONUCCI, *The compressive properties of single osteons*, Anat. Record, Vol.164, pp.377-390, 1968.

13. A. ASCENZI and E. BONUCCI, *The shearing properties of a single osteons*, Anat. Record, Vol.172, pp.499-510, 1972.

14. A. ASCENZI and E. BONUCCI, *Relationship between ultrastructure and "pin test" in osteons*, Clin. Orthop. Vol.121, pp.175-254, 1976.

15. A. ASCENZI, E. BONUCCI and A.CHECCUCCI, *The tensile properties of single osteons studied using a microwave extensimeter*, [in] Studies on the Anatomy and Function of Bone and Joints, F.G. Evans [ed.], pp.121-141, Springer-Verlag, Berlin 1966.

16. A. ASCENZI, E. BONUCCI and A. SIMKIN, *An approach to the mechanical properties of single osteon lamellae*, J. Biomech., Vol.6, pp.227-235, 1973.

17. A. ASCENZI, A. BOYDE, P. BIANKO, and M. PORTIGLIATI BARBOS, *Relationship between mechanical properties and structure in secondary bone*, Connective Tissue Res., Vol.15, pp.73-76, 1986.

18. A. ASCENZI, A. BOYDE, M. PORTIGLIATTI BARBOS and S. CARAMDO, *Micro-biomechanics vs macro- biomechanics in cortical bone. A micromechanical investigation of femurs deformed by bending*, J. Biomech., Vol.20, pp.1045-1053, 1987.

19. G.A. BAKER, *Essentials of Padé Approximants*, Academic Press, London 1975.

20. G.A. BAKER and P. GRAVES-MORRIS, *Padé Approximants*, [in] Gian-Carlo Rota, [ed.], Encyclopedia of Mathematics and its Applications, Vol.59, Cambridge University Press 1996.

21. G. S. BEAUPRE and W.C. HAYES, *Finite element analysis of a three dimensional opened-celled model for trabecular bone*, J. Biomech. Engng., Vol.107, pp.249-256, 1985.

22. M.P. BENDSØE and N. KIKUCHI, *Generating optimal topologies in structural design using a homogenization method*, Commun. Mech. appl. Mech. Enging., Vol.71, pp.192-224, 1988.

23. D.J. BERGMAN, *The dielectric constant of a composite material- A problem in classical physics*, Phys. Report., Vol.C43, pp.377-407, 1978.

24. M.P. BENDSØE, *Optimization of Structural Topology, Shape, and Material*, Springer-Verlag, Berlin 1995.

25. A. BENSOUSSAN, J.L. LIONS, and G. PAPANICOULAOU, *Asymptotic Analysis for Periodic Structures*, North- Holland, Amsterdam 1978.

26. R.M. CHRISTENSEN, *Mechanics of Composite Materials*, John Wiley&Sons, New York, 1979.

27. D. CIORANESCU and J. SAINT JEAN PAULIN, *Homogenization of Reticulated Structures*, Springer, New York 1999.

28. D. CIORANESCU and J. SAINT JEAN PAULIN, *Asymptotic analysis of elastic wireworks*, Laboratoire d'analyse numérique, Université Paris VI, R89008, 1989.

29. S.C. COWIN, *The mechanical properties of cortical bone tissue*, [in] Bone Mechanics, S.C. Cowin [ed.], pp.97-127, CRC Press, Inc. Boca Raton, Florida 1989.

30. S.C. COWIN, *The mechanical properties of cancellous bone*, [in] Bone Mechanics, S.C. Cowin [ed.], pp.129-157, CRC Press, Inc. Boca Raton, Florida 1989.

31. S.C. COWIN [ED.], *Bone Mechanics Handbook*, CRC Press, Boca Raton 2001.

32. J.M. CROLET , *Homogenization: mathematical method applied to haversian cortical bone structure*, Proceedings 1st World Congress of Biomechanics, pp.156-172, 1990.

33. J.M. CROLET, B. AOUBIZA and A. MEUNIER, *Compact bone: numerical simulation of mechanical characteristics*, J. Biomech., Vol.26, 6, pp.677-687, 1993.

34. P. FRASCA, *Structure and mechanical properties of human single osteons*, PH.D. thesis, Rensselear Polytechnic Institute, Troy, N,Y. 1974.

35. P. FRASCA and R. A. HARPER, *Isolation of a single osteons and osteon lamellae*, Acta Anat., Vol.95, pp.122-129, 1977.

36. A. GAŁKA, B. GAMBIN J.J. TELEGA and S. TOKARZEWSKI, *Macroscopic properties of compact bone and its hierarchical structure*, Acta Bioeng. Biomech., Vol.5, Suplement 1, pp.155-160, 2003.

37. A. GAŁKA, J.J TELEGA and S. TOKARZEWSKI , *Application of homogenization to evaluation of effective moduli of linear elastic trabecular bone with plate-like structure*, Arch. Mech., Vol.51, pp.335-355, 1999.

38. J.L. GIBSON, *The mechanical behaviour of cancellous bone*, J. Biomechanics, Vol.18, pp.317-328, 1985.

39. L.J. GIBSON, M.F. ASHBY, *Cellular solids*, Pergamon Press, New York 1988.

40. L.J. GIBSON, M.F. ASHBY, J, ZHANG and T.C. TRIANTAFILLOU, *Failure surfaces for cellular materials under multiaxial loads - II. Comparison of models with experiment*, Int. J. Mech, Sci., Vol, 31, pp.665-678, 1989.

41. K.GOLDEN and G. PAPANICOLAOU, *Bounds for effective parameters of heterogeneous media by analytic continuation*,Comm.Math.Phys., Vol.90, pp.473-491, 1983.

42. S. HENGSBERGER, J, ENSTOEM, F. PEYRIN and PH. ZYSSET, *How is the indentation modulus of bone tissue related to its macroscopic elastic response? A validation study*, J. Biomech., Vol.36, pp.1503-1509, 2003.

43. J. HOHE and W. BECKER, *Effective stress-strain relations for two-dimensional celluar sandwich cores: Homogenization, material models and properties*, Appl. Mech, Reviews, Vol.55, pp.61-87, 2002.

44. S.J. HOLLISTER, J.M. BRENNAN and N. KIKUCHI , *A homogenization sampling procedure for calculating trabecular bone effective stiffness and tissue level stress*, J. Biomech., Vol.4, 27, pp.433-444, 1994.

45. S.J. HOLLISTER, D.P. FYHIRE, K.J. JEPSEN and S.A. GOLDSTEIN , *Application of homogenization theory to the study of trabecular bone mechanics*, J. Biomech., Vol.24, 9, pp.825-839, 1991.

46. S. JEMIOŁO and J.J. TELEGA, *Fabric tensors in bone mechanics*, Engng. Trans., Vol.46, pp.3-26, 1998.

47. S. JEMIOŁO and J.J. TELEGA, *Fabric tensors in bone mechanics: constitutive relationships and strength criteria*, this volume.

48. M. KASRA and M.D.GRYNPAS, *Static and dynamic finite element analyses of an idealized structural model of vertebral trabecular bone*, J. Biomech. Eng., Vol.120, pp.267-272, 1998.

49. J.L. KATZ , *Hierarchical modeling of compact bone as a fiber reinforced material*, in: Advances in Bioengineering, R.E. Mates and C.R Smith [ed.], pp.18-19, American Society of Mechanical Engineers, New York 1976.

50. R.V. KOHN and G. STRANG, *Optimal design and relaxation of variational problems, I, II, III*, Comm. Pure Appl. Math., Vol.39, pp.113-137, 139-182, 353-377, 1986.

51. P. KOWALCZYK, *Elastic properties of cancellous bone derived from finite element models of parametrized microstructure cell*, J. Biomech., Vol.36, pp.961-972, 2003.

52. T. LEWIŃSKI and J.J. TELEGA, *Plates, Laminates and Shells: Asymptotic Analysis and Homogenization*, World Scientific, Singapore 2000.

53. G LOWET, P. RÜEGSEGGER, H. WEINANS and A. MEUNIER ,[Eds.], *Bone Research in Biomechanics*, IOS Press, Amsterdam 1997.

54. K.A. LURIE, A.V. FEDOROV and A.V. CHERKAEV , *Regularization of optimal design problems for bars and plates, I and II* , J. Opt. Theory Appl., Vol.37, pp.499-543, 1982.

55. J. MCELHANEY, N. ALEM and V. ROBERTS, *A porous block model for cancellous bones*, ASME Publication Vol.70-WA/BHF-2, pp.1-9, 1970.

56. T.L.A. MOORE and L.J. GIBSON, *Modeling modulus reduction in bovine trabecular bone damaged in compression*, J. Biomech. Eng., Vol.123, pp.613-622, 2001.

57. R. MÜLLER and P. RÜEGSEGGER, *Micro-tomographic imaging for the nondestructive evaluation of trabecular bone architecture*, [in] Bone Research in Biomechanics, G. Lowet, P. Rüegsegger, H. Weinans and A. Meunier [Eds.], pp.61-79, IOS Press, Amsterdam 1997.

58. W. NOWACKI, *Teoria sprężystości (Theory of Elasticity)*, Państwowe Wydawnictwo Naukowe, Warszawa 1970, in Polish.

59. N. OHNO, D. OKUMURA and H. NOGUCHI, *Microscopic symmetric bifurcation condition of cellular solids based on a homogenization theory of finite deformation*, J. Mech. Phys. Solids, Vol.50, pp.1125-1153, 2002.

60. N. OHNO, D. OKUMURA and H. NOGUCHI, *Microscopic buckling and macroscopic instability of periodic cellular solids*, ICM-9, Genève, May 26-29, 2003.

61. D. OKUMURA, N. OHNO and H. NOGUCHI, *Post-buckling analysis of elastic honeycombs subject to in-plane biaxial compression*, Int. J. Solids Structures, Vol.39, pp.3487-3503, 2002.

62. D.W. OVERAKER, A.M. CUITIÑO and N.A. LANGRANA, *Effects of morphology and orientation on the behavior of two-dimensional hexagonal foams and application in a re-entrant foam anchor model*, Mech. Mater., Vol.29, pp.43-52, 1998.

63. W.M. PAYTEN, B. BEN-NISSAN and D.J. MERCER, *Optimal topology design using global self-organisational approach*, Int. J. Solids Structures, Vol.35, pp.219-237, 1998.

64. W.T.PERRINS, D.R. MCKENZIE and R.C. MC PHEDRAN, *Transport properties of regular array of cylinders*, Proc. R. Soc. Lond. Vol.A 369, pp.207-225, 1979.

65. M. PORTIGLIATTI BARBOS, P. BIANCO, A. ASCENZI and A. BOYDE , *Collagen orientation in compact bone: II. Distribution of lamellae in whole of the human femoral shaft with reference to its mechanical properties*, Metal. Bone Dis. &Rel. Res., Vol.5, pp.309-315, 1984.

66. J.W. PUGH, R.M. ROSE and E.L. RADIN , *A structural model for the mechanical behavior of trabecular bone*, J. Biomech., Vol.6, pp.657-670, 1973.

67. A.P. ROBERTS, *Morphology and thermal conditivity of model organic aerogels*, Phys. Rev. E, Vol.55, pp.1286-1289, 1997.

68. A.P. ROBERTS and M.A. KNACKSTEDT, *Mechanical and transport properties of model foamed solids*, J. Mater. Sci. Letters, Vol.14, pp.1357-1359, 1995.

69. E. SANCHEZ- PALENCIA, *Non- Homogeneous Media and Vibration Theory*. Springer, Berlin 1980.

70. G. SHI and P. TONG, *The derivation of equivalent constitutive equations of honeycomb structure by a two scale method*, Comp. Mech., Vol.15, pp.395-407, 1995.

71. J.W. SMITH, *The arrangement of collagen fibers in human secondary osteons*, J. Bone Joint Surgery, Vol.42B, p.588, 1960.

72. P.M. SUQUET, *Elements of homogenization theory for inelastic solid mechanics*, [in] Homogenization Techniques for Composite Media, (E. Sanchez- Palencia and A. Zaoui [Eds.]), Springer, Berlin 1985.

73. J.J. TELEGA, *Stochastic homogenization: convexity and nonconvexity*, [in] Nonlinear Homogenization and its Applications to Composites, Polycrystals and Smart Materials, P.Ponte Castañeda, J.J. Telega and B. Gambin [eds.], Kluwer, 2004, in press.

74. J.J. TELEGA and W. BIELSKI, *Flow in random porous media: effective models*, Computers and Geotech., Vol.30, pp.271-288, 2003.

75. J.J. TELEGA, A GAŁKA and S. TOKARZEWSKI , *Effective moduli of trabecular bone*, Acta Bioeng. Biomech., Vol.1, pp.53-57, 1999.

76. J.J. TELEGA, A GAŁKA and S. TOKARZEWSKI , *Application of the reiterated homogenization to determination of effective moduli of compact bone*, J. Theor. Appl. Mech., Vol.37, pp.687-706, 1999.

77. J.J. TELEGA, S. TOKARZEWSKI and A GAŁKA, *Hydraulic stiffening of cancellous bone due to the presence of marrow: The application of multipoint Padé approximants*, Ukrainian- Polish Conference, "Theoretical Foundation of Civil Engineering", (W. Szcześniak [ed.]), OW PW, pp.331-338, Warszawa 2000.

78. J.J. TELEGA, S. TOKARZEWSKI and A.GAŁKA *Modelling torsional properties of human bones by multipoint Padé approximants.* In Numerical Analysis and Its Application (L. Vulkov, J. Waśniewski, and P. Yalamov [Eds.]), Springer-Verlag, pp. 741–748, Berlin 2001.

79. P. THEOCARIS, *The influence of porosity on the failure behaviour of foams*, Int. J. Damage Mech., Vol.7, pp.301-331, 1998.

80. S. TOKARZEWSKI *N- point Padé approximants to real valued Stieltjes series with nonzero radii of convergence*, J. Comp. Appl. Math., Vol.75, pp.259-280, 1996.

81. S. TOKARZEWSKI, *Two- point Padé approximants for the expansion of Stieltjes functions in a real domain*, J. Comp. Appl. Math., Vol.67, pp.59-72, 1996.

82. S. TOKARZEWSKI , A.GAŁKA and I. ANDRIANOV, *Bounds on the effective transport coefficients of two- phase media from discrete theoretical and experimental data*, Comp. Assis. Mech. and Eng. Sc., Vol.4, pp.229- 241, 1997.

83. S. TOKARZEWSKI, A. GAŁKA and J.J. TELEGA, *Cancellous bone as a cellular solid: the determination of effective material properties*, [in] Proc. Conf. on Biomechanics: Modelling, Computational Methods, Experiments and Biomedical Applications, (J. Awrejcewicz, M. Ciach and M. Kleiber [Eds.]), pp.191-196, Technical University of Łódź, (in Polish), 1998.

84. S. TOKARZEWSKI and J.J. TELEGA, *Inequalities for two- point Padè approximants to the expansions of Stieltjes functions in a real domain*, Acta Applic. Math., Vol.48, pp.285-297, 1997.

85. S. TOKARZEWSKI and J.J. TELEGA, *S- continued fraction method for the investigation of a complex dielectric constant of two- phase composite*, Acta Appl. Math., Vol.49, pp.55-83, 1997.

86. S. TOKARZEWSKI , J.J. TELEGA and A. GAŁKA, *A contribution to evaluation of effective moduli of trabecular bone with rod-like microstructure*, J. Theor. Appl. Mech., Vol.3, 37, pp.707-728, 1999.

87. S. TOKARZEWSKI , J.J. TELEGA and A. GAŁKA , *Torsional rigidities of cancellous bone filled with marrow: The application of multipoint Padé approximants*, Eng. Trans., Vol.49, pp.135-153, 2001.

88. S. TOKARZEWSKI, J.J. TELEGA, and A. GAŁKA, *Prediction of torsional rigidities of bone filled with marrow: The application of one-point Padé approximants,* Acta Bioeng. Biom., vol.2, 1, pp.560-566, 2000.

89. S. TOKARZEWSKI, J.J. TELEGA, and A. GAŁKA, *Badanie własności mechanicznych belek porowatych modelujących własności kości*, Cieplne Maszyny Przepływowe , vol. 117, pp.329–335, 2000.

90. S. TOKARZEWSKI, J.J. TELEGA, AND A. GAŁKA, *A study of hydraulic stiffening of a cancellous bone filled with marrow*, Acta Bioeng. Biomech., Vol.3, 2, pp.585–593, 2001.

91. T.C. TRIANTAFILLOU, J. ZHANG, T.L. SHERCLIFF, L.J. GIBSON and M.F. ASHBY, *Failure surfaces for celluar materials under multiaxial loads - I, Modelling*, J. Mech. Sci., Vol.31, pp.639-663, 1989.

92. D. ULRICH, T. HILDEBRAND, B. VAN RIETBERGEN, R. MÜLLER and P. RÜEGSEGGER, *The quality of trabecular bone evaluated with micro-computed tomography, FEA and mechanical testing*, [in] Bone Research in Biomechanics, (G. Lovet, P. Rüegsegger, H. Weinans and A. Meunier [Eds.]), pp.97-112, IOS Press, Amsterdam 1997.

93. S. VAJJHALA, A.M. KRAYNIK and L.J. GIBSON, *A cellular solid model for modulus reduction due to resorphion of trabeculae in bone*, J. Biomech. Eng., Vol.122, pp.511-515, 2000.

94. R. VANDERBY and P.P. PROVENZANO, *Collagen in connective tissue: from tendon to bone*, J. Biomech., Vol.36, pp.1523-1527, 2003.

95. W.E. WARREN and A.M. KRAYNIK, *Linear elastic behavior of a low-density Kelvin foam with open cells*, J. Appl. Mech., Vol.64, pp.787-794, 1997.

96. J.L. WILLIAMS and J.L. LEWIS, *Properties and anisotropic model of cancellous bone from the proximal tibia epiphysis*, J. Biomech. Engng., Vol.104, pp.50-56, 1982.

97. P.K. ZYSSET, R.W. GOULET and S.J. HOLLISTER, *A global relationship between trabecular bone morfology and homogenized elasic properties*, J. Biomech. Eng., Vol.12, pp.640-646, 1998.

98. H.S. YOON and J.L. KATZ, *Measurements of elastic properties and micro-hardness*, J. Biomech., Vol.9, p.459, 1976.